

# Contribution of Organic Nitrates to Organic Aerosol over South Korea during KORUS-AQ

Hannah S. Kenagy, Paul S. Romer Present, Paul J. Wooldridge, Benjamin A. Nault, Pedro Campuzano-Jost, Douglas A. Day, Jose L. Jimenez, Azimeh Zare, Havaala O.T. Pye, Jinhyeok Yu, Chul H. Song, Donald R. Blake, Jung-Hun Woo, Younha Kim, and Ronald C. Cohen\*



Cite This: <https://doi.org/10.1021/acs.est.1c05521>



Read Online

ACCESS |

Metrics & More

Article Recommendations

Supporting Information

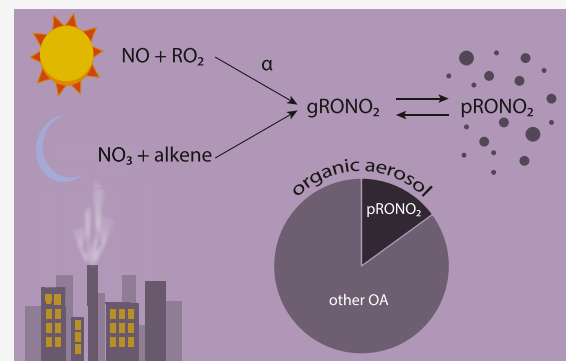
**ABSTRACT:** The role of anthropogenic  $\text{NO}_x$  emissions in secondary organic aerosol (SOA) production is not fully understood but is important for understanding the contribution of emissions to air quality. Here, we examine the role of organic nitrates ( $\text{RONO}_2$ ) in SOA formation over the Korean Peninsula during the Korea–United States Air Quality field study in Spring 2016 as a model for  $\text{RONO}_2$  aerosol in cities worldwide. We use aircraft-based measurements of the particle phase and total (gas + particle)  $\text{RONO}_2$  to explore  $\text{RONO}_2$  phase partitioning. These measurements show that, on average, one-fourth of  $\text{RONO}_2$  are in the condensed phase, and we estimate that  $\approx 15\%$  of the organic aerosol (OA) mass can be attributed to  $\text{RONO}_2$ . Furthermore, we observe that the fraction of  $\text{RONO}_2$  in the condensed phase increases with OA concentration, evidencing that equilibrium absorptive partitioning controls the  $\text{RONO}_2$  phase distribution. Lastly, we model  $\text{RONO}_2$  chemistry and phase partitioning in the Community Multiscale Air Quality modeling system. We find that known chemistry can account for one-third of the observed  $\text{RONO}_2$ , but there is a large missing source of semivolatile, anthropogenically derived  $\text{RONO}_2$ . We propose that this missing source may result from the oxidation of semi- and intermediate-volatility organic compounds and/or from anthropogenic molecules that undergo autoxidation or multiple generations of OH-initiated oxidation.

**KEYWORDS:** organic nitrates, organic aerosol, urban air quality, aerosols, particulate matter, volatile organic compounds, nitrogen oxides, absorptive partitioning theory

## 1. INTRODUCTION

Organic aerosol (OA) constitutes a large, and often dominant, fraction of tropospheric aerosol mass.<sup>1–3</sup> Much of this OA is secondary (secondary OA, SOA), produced from volatile organic compounds (VOCs) that are sufficiently oxidized in the atmosphere to be condensable and/or water-soluble.<sup>4–8</sup> The chemical and physical processes that control SOA production, however, are complex and currently highly uncertain.<sup>1,9–16</sup>

Particle-phase organic nitrates (p $\text{RONO}_2$ ) have recently emerged as a significant component of SOA in areas dominated by biogenic emissions, including in the Southeast United States,<sup>17–22</sup> in the Rocky Mountains,<sup>23</sup> across Europe,<sup>24</sup> in the boreal forest,<sup>25</sup> in the California Central Valley,<sup>26,27</sup> and in rural areas of both northern and southern China.<sup>28–30</sup> A number of studies have also found significant contributions of p $\text{RONO}_2$  to SOA in regions of oil and gas production, including in the Alberta Oil Sands<sup>31</sup> and in the Uintah Basin.<sup>32</sup> Recent observations have shown that organic nitrates are a significant contributor to OA in Chinese cities.<sup>33,34</sup> Specifically, Yu et al.<sup>34</sup> found that organic nitrates



make up 9–25% of OA during spring-autumn in urban Shenzhen, and the dominant precursors to p $\text{RONO}_2$  included both biogenic ( $\alpha$ -pinene, limonene, and camphene) and anthropogenic (styrene) VOCs.

Organic nitrates are produced from the oxidation of VOCs in the presence of  $\text{NO}_x$  ( $\equiv \text{NO} + \text{NO}_2$ ), as shown in Figure 1. During the daytime when photochemistry is active, the OH oxidation of VOCs generates  $\text{RO}_2$  radicals (R1). The minor products (branching ratio  $\alpha$ ) of the reaction of NO with  $\text{RO}_2$  radicals are gas-phase organic nitrates (g $\text{RONO}_2$ , R2). In the nocturnal residual layer away from fresh NO emissions,  $\text{NO}_3$  radicals can add to the double bonds of alkenes to generate g $\text{RONO}_2$  (R3), for example, ref 35.

Received: August 19, 2021

Revised: November 18, 2021

Accepted: November 22, 2021

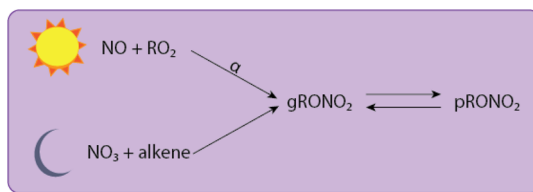


**Figure 1.** Schematic of  $\text{RONO}_2$  production and phase partitioning.



If an  $\text{RONO}_2$  molecule generated from either the OH-initiated or  $\text{NO}_3$ -initiated reaction pathways has sufficiently low volatility, it may partition into the aerosol phase as a particle-phase organic nitrate,  $\text{pRONO}_2$  (Figure 1). At 273 K, the addition of a nitrate functional group reduces the saturation concentration of a given molecule by 2.23 orders of magnitude,<sup>36</sup> thereby generating a lower volatility compound that may condense to form SOA.

In this study, we examine the contribution of  $\text{pRONO}_2$  to OA in Seoul, Korea. As a megacity, Seoul has a complex mixture of urban emissions, including from a number of chemical facilities and from the transport of emissions from China, that contribute to the aerosol burden,<sup>37,38</sup> although the dominant precursors for SOA production in Seoul are locally emitted VOCs.<sup>37</sup> To better understand the sources of SOA in Seoul, here we aim to quantify the contribution of  $\text{pRONO}_2$  to the total OA mass and determine the precursors and processes that control the production of  $\text{pRONO}_2$  in Korea using observations from the 2016 Korea–United States Air Quality (KORUS-AQ) measurement campaign.

## 2. METHODS

Here, we introduce the KORUS-AQ campaign (Section 2.1), the UC Berkeley thermal dissociation laser-induced fluorescence (TD-LIF) measurements of  $\text{pRONO}_2$  (Section 2.2), the University of Colorado Boulder high-resolution time-of-flight aerosol mass spectrometer (CU-AMS) measurements of

$\text{pRONO}_2$  and OA (Section 2.3), and our Community Multiscale Air Quality (CMAQ) modeling system simulations of  $\text{RONO}_2$  over Northeast Asia during the time period of the KORUS-AQ campaign (Section 2.4).

**2.1. KORUS-AQ.** The KORUS-AQ campaign took place during May and June 2016 over the Korean Peninsula and the Yellow Sea.<sup>39</sup> Seoul, Korea, is bordered to the west by the Yellow Sea and Gyeonggi Bay and bordered to the north, east, and south by forested and mountainous regions.<sup>40</sup> During KORUS-AQ, winds were typically from the west or northwest, meaning that air over the Yellow Sea can be considered “background” air for Seoul.<sup>41</sup> There are a number of large industrial facilities along the northwest coast of South Korea, including the Daesan petrochemical complex which produces large amounts of VOC emissions.<sup>42</sup>

This analysis uses observations from the NASA DC-8 which flew 20 research flights out of Pyeongtaek, South Korea ( $\approx 60$  km south of Seoul). Flights typically began around 08:00 LT (KST). During a typical flight, three missed approaches were performed over the Seoul Air Base (within 15 km of the Seoul city center): one soon after takeoff around 08:00 LT, one around 12:00 LT, and one prior to landing around 15:00 LT. Each missed approach included 15–45 min of observations within the boundary layer in the Seoul metropolitan area. Flights also consisted of transects west of Seoul over the Yellow Sea, south of Seoul to Jeju, and/or southeast of Seoul to Busan at varying altitudes, as shown in Figure 2. We use 60 s measurement averages in this analysis.

During KORUS-AQ, the NASA DC-8 was equipped with the only two currently aircraft certified techniques to measure total  $\text{pRONO}_2$ : the UC Berkeley TD-LIF instrument and the University of Colorado Boulder CU-AMS. Although some other measurement techniques exist to measure certain specific  $\text{RONO}_2$  species, for example, refs 43 and 44, the TD-LIF and CU-AMS measurement schemes allow for measurements of the sum of all  $\text{pRONO}_2$  species.

**2.2. TD-LIF Measurements of tRONO<sub>2</sub> and pRONO<sub>2</sub>.** Measurements of tRONO<sub>2</sub> (gas + particle) were made using the UC Berkeley TD-LIF instrument.<sup>45,46</sup> Briefly, one channel of the instrument measures  $\text{NO}_2$  by LIF. In two other channels, air flows through a heated quartz oven prior to LIF

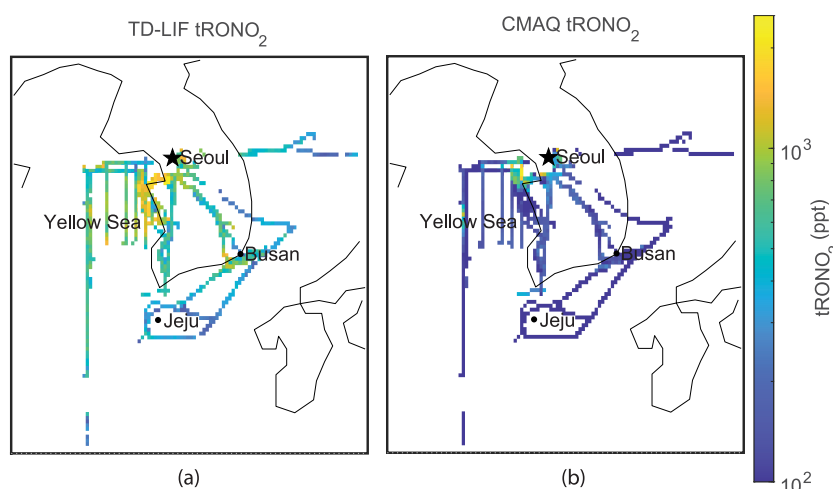


**Figure 2.** Maps of average (a) TD-LIF measured and (b) CMAQ-modeled tRONO<sub>2</sub> on a log scale, gridded to  $0.1^\circ$ . Seoul, Jeju, Busan, and the Yellow Sea are labeled for reference. Note that the modeling domain is larger than the domain of the map plotted here and covers much of Northeast Asia ( $17.4$ – $47.2^\circ$  N and  $93.2$ – $147.4^\circ$  E).

detection of  $\text{NO}_2$ . One channel's oven is set at 180 °C, the temperature at which peroxy nitrates ( $\text{RO}_2\text{NO}_2$ ) dissociate into  $\text{RO}_2$  and  $\text{NO}_2$ . The second is set at 360 °C, the temperature at which  $\text{RONO}_2$  dissociate into  $\text{RO} + \text{NO}_2$ . The difference in  $\text{NO}_2$  detected in adjacent channels gives the mixing ratio for each class of compounds: the  $\text{RO}_2\text{NO}_2$  mixing ratio corresponds to the difference between the 180 °C channel and the unheated channel, and the  $\text{RONO}_2$  mixing ratio corresponds to the difference between the 360 °C channel and the 180 °C channel.

$\text{pRONO}_2$  concentrations were measured using a fourth channel configured as described in Rollins et al.<sup>47</sup> Before entering the heated section of the instrument, air passes through a 10 cm long activated carbon honeycomb denuder with an outer diameter of 2 cm, which removes gas-phase compounds (MAST Carbon International Ltd. carbon monolith with 89 cells  $\text{cm}^{-2}$  where each open square is 0.63 by 0.63 mm with 0.43 mm thick walls in between). The particles that remain are then rapidly heated to vaporize the aerosols and dissociate the  $\text{RONO}_2$  molecules present into  $\text{RO}$  and  $\text{NO}_2$ .  $\text{NO}_2$  is then detected via LIF, giving a measurement of  $\text{pRONO}_2$ . We estimate a limit of detection of 20 ppt of  $\text{pRONO}_2$  or 0.055  $\mu\text{g m}^{-3}$  of  $\text{NO}_3^-$ . Although inorganic nitrate compounds will also be vaporized, volatile inorganic nitrate salts form  $\text{HNO}_3$  when vaporized<sup>48</sup> and will therefore not interfere in this measurement. Empirical and theoretical studies confirm that  $\text{NO}_2$ ,  $\text{HNO}_3$ , and gas-phase organic nitrates are all removed at nearly 100% efficiency in the charcoal denuder, while particles greater than 100 nm in diameter are transmitted with over 95% efficiency.<sup>47</sup> A recent work has shown that  $\text{HONO}$  is removed with near-100% efficiency in dry air and with 85% efficiency at an RH of 46% with a similar denuder.<sup>49</sup> Furthermore, during KORUS-AQ, the denuder could be bypassed with a pair of three-way valves, as shown in Figure S1. When bypassed, the  $\text{NO}_2$  calibration mixture reached the  $\text{pRONO}_2$  LIF cell. When not bypassed, the  $\text{NO}_2$  calibration events served as checks for  $\text{NO}_2$  breaking through the denuder. Compared to the 20 ppt limit stated above, no breakthroughs of the 12 or 24 ppb  $\text{NO}_2$  calibration steps were detectable during the deployment, as shown in Figure S6.

KORUS-AQ is the first time  $\text{pRONO}_2$  measurements have been made with TD-LIF on aircraft. Previous ground-based measurements of  $\text{pRONO}_2$  by TD-LIF were made in the Rocky Mountains during BEACHON-RoMBAS in 2011,<sup>23</sup> in the Uintah Basin during the 2012 Uintah Basin Winter Ozone Study (UBWOS),<sup>32</sup> in the Southeast United States during Southern Oxidant and Aerosol Study (SOAS) in 2013,<sup>21</sup> and in the California Central Valley during CalNex in 2010.<sup>27</sup>

We apply a small correction for the loss of charged particles to TD-LIF measurements of  $\text{tRONO}_2$  and  $\text{pRONO}_2$ . In the TD-LIF inlet configuration during KORUS-AQ, air for all channels goes through 10–20 cm of PFA Teflon before heating. We performed a series of laboratory experiments (detailed in Section S1) to determine the loss of charged particles in these lengths of PFA Teflon tubing. Taking into account the ambient distribution of charged particles<sup>50</sup> and the observed aerosol size distribution measured during KORUS-AQ, there is less than 20% loss for charged particles with diameters less than 280 nm in the TD-LIF inlet.

We also apply a correction for inertial losses of particles in the TD-LIF inlet. We model the inertial losses on the two bends (90 and 98°) in the inlet (see Section S1) for varying particle sizes. We apply the size-dependent modeled losses to

the aerosol volume distribution measured by a laser aerosol spectrometer (Langley LARGE Group). On average, we estimate that TD-LIF observes ≈60% of the particles observed by laser aerosol spectrometry. We apply both particle loss corrections (charged and inertial) to both the  $\text{pRONO}_2$  and  $\text{tRONO}_2$  TD-LIF measurements.

**2.3. CU-AMS Measurements of  $\text{pRONO}_2$ .** A second measurement of  $\text{pRONO}_2$  was made by CU-AMS (Aerodyne Research, Inc.). CU-AMS also measured OA concentrations. A description of the CU-AMS aircraft sampling can be found in DeCarlo et al.,<sup>51</sup> Canagaratna et al.,<sup>52</sup> and Nault et al.<sup>37</sup>

The CU-AMS uses  $\text{NO}_x$  ion ratios ( $\text{NO}_2^+/\text{NO}^+$ ) to differentiate between inorganic nitrate ( $\text{NH}_4\text{NO}_3$ ) and organic nitrate ( $\text{pRONO}_2$ ),<sup>23,53</sup> described further in Section S2. Uncertainties in this method are greatest when  $\text{pRONO}_2 < 20\%$  of the total measured aerosol nitrate; those CU-AMS measurements have been removed from this analysis. This ion ratio technique has been used previously in rural environments where VOCs are dominantly biogenic and  $\text{RONO}_2$  concentrations are relatively small.<sup>17,23,54</sup> However, the high  $\text{NH}_4\text{NO}_3$  loadings in the urban environment measured during KORUS-AQ create uncertainty for the CU-AMS measurement of  $\text{pRONO}_2$ .

Although we applied a series of corrections for particle loss in the TD-LIF inlet (described in Section 2.2), we could not entirely reconcile the differences between the two measurements. Since the two measurements may be prone to larger uncertainties under different aerosol size and composition conditions, we conduct the following analyses using both the TD-LIF and CU-AMS  $\text{pRONO}_2$  measurements separately and treat them as upper and lower bounds. A comparison of the TD-LIF and CU-AMS measurements, both before and after applied corrections, can be seen in Figure S9.

Because the TD-LIF and CU-AMS  $\text{pRONO}_2$  measurements do not agree perfectly, we also use a CU-AMS-adjusted  $\text{tRONO}_2$  to ensure a consistent comparison. In the following calculations that use CU-AMS  $\text{pRONO}_2$ , we subtract the TD-LIF  $\text{pRONO}_2$  measurement from the TD-LIF  $\text{tRONO}_2$  measurement to give an estimate of the  $\text{gRONO}_2$  measured by TD-LIF. We then add the CU-AMS  $\text{pRONO}_2$  to the estimated TD-LIF  $\text{gRONO}_2$  to generate the CU-AMS-adjusted  $\text{tRONO}_2$ .

**2.4. CMAQ Modeling of  $\text{RONO}_2$  Chemistry and Phase Partitioning.** We ran the CMAQ model v5.2<sup>55,56</sup> with the RACM2\_Berkeley2.1 chemical mechanism<sup>22,57</sup> over Northeast Asia with a 15 km horizontal grid (17.4–47.2° N and 93.2–147.4° E) and 27 vertical layers. Meteorological fields were generated by WRF v3.8.1 and processed for use in CMAQ by MCIP v4.5.<sup>58</sup> The simulation period was April 17, 2016–June 12, 2016, with the first 14 days as a spin-up period to minimize the impact of initial conditions.

We used the KORUSv5.0 anthropogenic emission inventory developed at Konkuk University based on the CREATE emission inventory<sup>59</sup> which includes area, point, mobile, and ship emissions, MEGANv2.1 biogenic emissions,<sup>60</sup> and FINNv1.5 fire emissions,<sup>61</sup> all processed through the Sparse Matrix Operator Kernel Emission (SMOKE) system.<sup>62</sup> The KORUSv5.0 emission inventory was prepared using the SAPRC07T AERO6 mechanism, which we then converted to RACM2\_Berkeley2.1 (detailed in Table S1).

We made a few adjustments to the emission inventory informed by a series of comparisons between CMAQ-modeled VOC concentrations and aircraft VOC measurements made

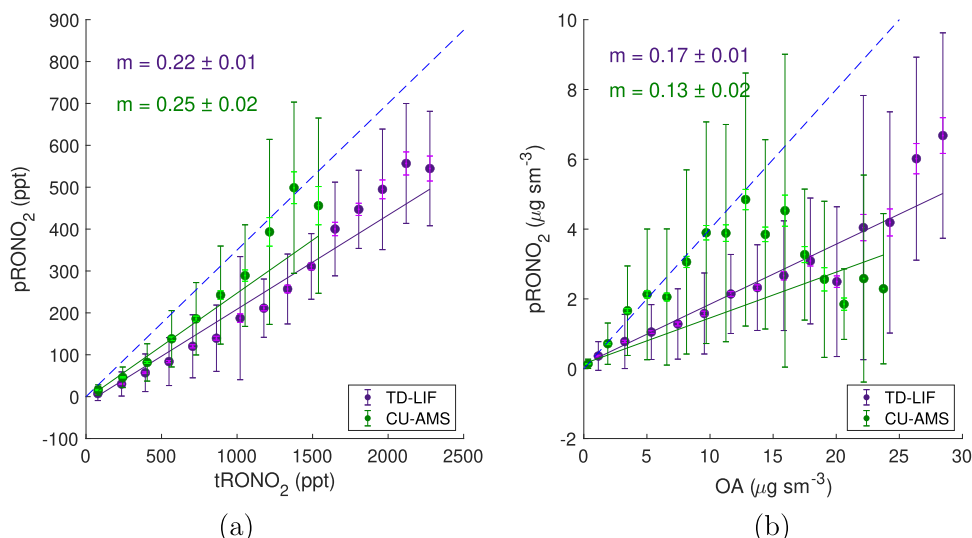


**Figure 3.** (a) Plot of pRONO<sub>2</sub> vs tRONO<sub>2</sub> mixing ratios as measured by TD-LIF and CU-AMS. Data are binned by the tRONO<sub>2</sub> mixing ratio, and the average pRONO<sub>2</sub> in each bin is plotted. The York fit shown corresponds to the average fraction of RONO<sub>2</sub> in the particle phase ( $F_p$ ). We draw an estimated upper limit ( $\approx 35\%$ ) for the fraction of RONO<sub>2</sub> in the particle phase, as shown in the blue dashed line, drawn above the mean of most measurements. (b) Plot of pRONO<sub>2</sub> mass concentration (using an estimated average molecular weight of 300 g mol<sup>-1</sup>) vs OA mass concentration. Data are binned by OA concentration, and the average pRONO<sub>2</sub> in each bin is plotted. The York fit shown corresponds to the average fraction OA mass that can be attributed to pRONO<sub>2</sub>. Again, we draw an estimated upper limit ( $\approx 40\%$ ) for the fraction of OA mass attributable to pRONO<sub>2</sub>, as shown in the blue dashed line, drawn above most measurement means. We do not understand why AMS data above 15  $\mu\text{g m}^{-3}$  deviate so strongly from the trend measured at lower OA concentrations. In both plots, the larger, dark-colored error bars correspond to the standard deviation of measurements within each bin to represent observed variability, whereas the smaller, light-colored error bars correspond to the standard error of measurements within each bin to represent measurement uncertainty. We apply a threshold requirement of 20 observations per bin to include in the plot.

with whole air samples analyzed with multicolumn gas chromatography.<sup>63</sup> We increased monoterpene emissions by a factor of 3 to improve the magnitude agreement between modeled and observed concentrations of monoterpenes (see Figure S12). Note that we expect monoterpenes in Korea to have both biogenic and anthropogenic sources.<sup>64,65</sup>

Comparison between modeled and observed BTEX (benzene, toluene, ethyl benzene, and xylenes) indicated that these species were also underestimated in the emission inventory (see Figure S12). We updated BTEX emissions over the Daesan petrochemical complex to match emission fluxes calculated from observations using a mass balance approach by Fried et al.<sup>42</sup> Elsewhere, we note that the spatial pattern of modeled TOL (defined as toluene and less-reactive aromatics, for measurement comparison purposes we approximate as the sum of toluene and ethyl benzene) corresponds well to the spatial pattern of the sum of measured toluene and ethyl benzene (see Figure S10). However, without any emission corrections, the model underestimates boundary layer TOL by a factor of 1.4. We also note that measurements of other reactive aromatics (xylenes and 1,2,4-trimethyl benzene) correlate well with the sum of measured toluene and ethyl benzene (see Figure S11). As such, we scale TOL emissions by 1.4 and define the emissions of the other reactive aromatics based on their measured ratios to the sum of toluene and ethyl benzene. We use measured *o*-xylene as a proxy for model species XYO, the sum of measured *m*-xylene and 1,2,4-trimethyl benzene as a proxy for model species XYM, and measured *p*-xylene as a proxy for model species XYP. This method results in setting XYO emissions as 0.05× TOL, XYM emissions as 0.08× TOL, and XYP emissions as 0.07× TOL, such that XYO, XYM, and XYP emissions all follow the same spatial pattern as TOL.

We use the default initial and boundary conditions from the ICON and BCON processors in CMAQ v5.2, respectively. However, measurements of isoprene-derived nitrates by Caltech's chemical ionization mass spectrometer (CIT-CIMS)<sup>66</sup> indicated that longer-lived propanone nitrate and ethanal nitrate were underestimated in CMAQ. Consequently, we increased the boundary and initial concentrations of propanone nitrate and ethanal nitrate to match the CIT-CIMS observations of both nitrates over the Yellow Sea (propanone nitrate = 21.5 ppt and ethanal nitrate = 4.1 ppt).

The original RACM2 (Regional Atmospheric Chemistry Mechanism)<sup>67</sup> is available in CMAQ v5.0.2 and later versions.<sup>68</sup> Browne et al.<sup>69</sup> modified the mechanism to RACM2\_Berkeley to expand the organic nitrate chemistry. New species, along with their corresponding oxidation rates and branching ratios, were added to further classify anthropogenic nitrates<sup>70–72</sup> and to represent monoterpene nitrates.<sup>73–76</sup> The parameterization of OH-initiated isoprene oxidation was also updated.<sup>77–79</sup> RACM2\_Berkeley was evaluated using aircraft observations over the Canadian boreal forest.<sup>69</sup>

RACM2\_Berkeley was updated to RACM2\_Berkeley2 in Zare et al.<sup>57</sup> to reflect recent advances in the representation of OH- and NO<sub>3</sub>-initiated BVOC oxidation under both low- and high-NO<sub>x</sub> conditions, with a focus on a detailed representation of nitrates derived from NO<sub>3</sub>-initiated oxidation of isoprene and on the fate of the most important individual biogenically derived organic nitrates. Deposition rates were also updated.

Zare et al.<sup>22</sup> revised RACM2\_Berkeley2 to RACM2\_Berkeley2.1 to include an explicit representation of multiphase organic nitrate formation and loss, including vapor-pressure-driven partitioning into OA, aqueous-phase uptake, and condensed-phase reactions. Further updates were also done

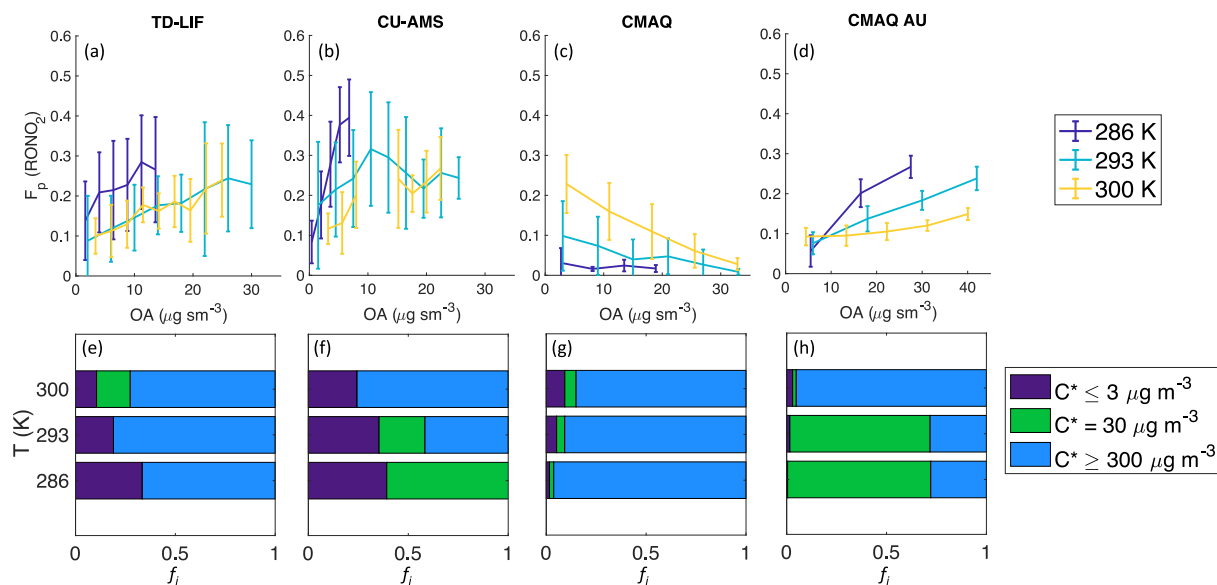


**Figure 4.** [Top] Plots of the fraction of RONO<sub>2</sub> in the particle phase ( $F_p$ ) vs OA concentration. Data were separated into three temperature bins (centered at 286, 293, and 300 K) and binned by OA concentration. The average  $F_p$  in each OA bin is plotted, and error bars represent the standard deviation of  $F_p$  in each bin. As suggested by absorptive partitioning theory, measured  $F_p$  increases with the increasing available solvating aerosol (in this case, OA). [Bottom] Temperature-dependent fractional distribution ( $f_j$ ) of saturation concentrations ( $C^*$ ) fit to a volatility basis set. Each set of plots is shown for the TD-LIF measurements (a,e), the CU-AMS measurements (b,f), unmodified CMAQ output (c,g), and CMAQ output with an unknown source of RONO<sub>2</sub> added (d,h).

to explicitly represent isoprene nitrates from NO<sub>3</sub> oxidation that are subject to reactive uptake to the aerosol phase. As such, the RACM2\_Berkeley2.1 mechanism represents our current understanding of RONO<sub>2</sub> chemistry and phase partitioning. Zare et al.<sup>22</sup> evaluated this mechanism (implemented in CMAQ) using observations from the SOAS campaign in the Southeast United States during Summer 2013. Inclusion of the particle-phase pathways for RONO<sub>2</sub> improved the model-measurement agreement for tRONO<sub>2</sub>, and the modeled fraction of tRONO<sub>2</sub> in the particle phase ( $F_p$ ) was within the range of observed  $F_p$ .

To compare modeled and measured concentrations, we sample CMAQ coincidentally in time (hourly resolution) and horizontal space with each observation. All comparisons in the following analysis use boundary-layer measurements (<1000 m) and the average of the bottom three model layers.

### 3. RESULTS

Maps of average TD-LIF measured and CMAQ modeled tRONO<sub>2</sub> used in the following analysis are shown in Figure 2. Both the measurements and model indicate that tRONO<sub>2</sub> concentrations are the highest in and around Seoul. However, the model consistently underpredicts tRONO<sub>2</sub> concentrations throughout the region. For reference, CMAQ predicts that >95% of pRONO<sub>2</sub> is derived from vapor-pressure-dependent partitioning into OA, whereas <5% of pRONO<sub>2</sub> enters the particle phase through aqueous pathways, similar to the study of Zare et al.<sup>22</sup> in the Southeast United States.

**3.1. RONO<sub>2</sub> Partition into the Aerosol Phase and Can Be a Significant Contribution to SOA.** We explore the average phase-partitioning behavior of RONO<sub>2</sub> during KORUS-AQ in Figure 3. Our observations from both TD-LIF and CU-AMS indicate that, on average, one-fourth of tRONO<sub>2</sub> is in the condensed phase and therefore contributes to the OA burden. We also consider a line, drawn above most measurement means in Figure 3, that represents a reasonable

upper limit of 35% for the fraction of tRONO<sub>2</sub> in the particle phase.

To quantify the contribution of pRONO<sub>2</sub> to the total OA concentration, we assume an average molecular weight for pRONO<sub>2</sub> of 300 g mol<sup>-1</sup>.<sup>27</sup> We expect condensable RONO<sub>2</sub> to be highly oxidized, to contain at least one nitrate group (molecular weight = 62 g mol<sup>-1</sup>), and to therefore have relatively high masses. With this assumption, we estimate that ≈15% of the OA mass can be attributed to pRONO<sub>2</sub>, as shown in Figure 3. Note that this estimate does not include CU-AMS measurements when pRONO<sub>2</sub> < 20% of the total measured aerosol nitrate. We again consider a reasonable upper limit, drawn above most measurement means, to estimate that a maximum of 40% of OA can be attributed to pRONO<sub>2</sub>. This is within the range of pRONO<sub>2</sub> contributions to OA mass measured across Europe (42%),<sup>24</sup> in a suite of studies across the eastern United States, western United States, and Europe (5–73%)<sup>80</sup> and in recent studies in urban and rural China (9–28%).<sup>34,81</sup>

**3.2. Observations Indicate That RONO<sub>2</sub> Phase Partitioning Is Controlled by Absorptive Partitioning into OA.** Previous studies have shown that vapor pressure controls the phase of organic nitrates.<sup>22,27</sup> This equilibrium absorptive partitioning follows Raoult's law: the fraction of RONO<sub>2</sub> in the particle phase increases with increasing mass of the absorbing or solvating aerosol, namely, total OA.<sup>82,83</sup> Accordingly, the equilibrium fraction of an individual RONO<sub>2</sub> species *i* in the particle phase ( $F_{p,i}$ ) is given by

$$F_{p,i} = \frac{C_{p,i}}{C_i} = \frac{C_{OA}/C_i^*(T)}{1 + C_{OA}/C_i^*(T)} = \left(1 + \frac{C_i^*(T)}{C_{OA}}\right)^{-1} \quad (1)$$

Here,  $C_{p,i}$  and  $C_i$  are the particle phase and total concentrations of species *i*, respectively.  $C_i^*(T)$  is the temperature-dependent saturation concentration ( $\mu\text{g m}^{-3}$ ) of species *i* and  $C_{OA}$  is the concentration of total OA.

**Table 1.** Comparison of the York Fit Slopes between Measured (by TD-LIF and CU-AMS) and CMAQ Modeled Concentrations of tRONO<sub>2</sub>, pRONO<sub>2</sub>, and F<sub>p</sub><sup>a</sup>

	tRONO <sub>2</sub>		pRONO <sub>2</sub>		F <sub>p</sub>	
	TD-LIF	CU-AMS	TD-LIF	CU-AMS	TD-LIF	CU-AMS
CMAQ	0.30	0.35	0.12	0.09	0.56	0.35
CMAQ add unknown	0.88	0.98	0.92	0.79	0.61	0.44

<sup>a</sup>Comparison is shown for both the unmodified CMAQ output and CMAQ output with an unknown source of condensable RONO<sub>2</sub> added. Scatter plots of these comparisons can be seen in Figure S14.

For both the TD-LIF and CU-AMS measurements of pRONO<sub>2</sub>, the fraction of RONO<sub>2</sub> in the particle phase ( $F_p$ ) increases with increasing OA concentration and increases with decreasing temperature, as shown in Figure 4. Assuming that the speciation of RONO<sub>2</sub> is invariant with temperature, these relationships between  $F_p$ , OA, and temperature indicate that the phase partitioning of RONO<sub>2</sub> during KORUS-AQ is indeed controlled by equilibrium absorptive partitioning.

To determine the volatility distribution of RONO<sub>2</sub> observed during KORUS-AQ, we define a saturation concentration basis set of  $\{C_j^*\} = \{3, 30, 300\} \mu\text{g m}^{-3}$ , following the convention of Donahue et al.<sup>82</sup> Although we expect some RONO<sub>2</sub> species to have volatilities outside of this range, because the OA concentrations we observe during KORUS-AQ do not exceed  $40 \mu\text{g m}^{-3}$ , we cannot reasonably constrain volatilities outside of this defined basis set. Given this basis set, the total fraction of organic nitrates in the particle phase ( $F_{p,\text{tot}}$ ) can be represented as

$$F_{p,\text{tot}} = \frac{\sum_i C_i F_{p,i}}{\sum_i C_i} = \sum_{j=1}^n f_j \left( 1 + \frac{C_j^*}{C_{\text{OA}}} \right)^{-1} \quad (2)$$

Here,  $f_j$  is the fraction of organic nitrates that can be classified as having saturation concentration  $C_j^*$  and  $n = 3$  for the basis set defined earlier.

We solve for each  $f_j$  in eq 2 using our observations of  $F_{p,\text{tot}}$  (=pRONO<sub>2</sub>/RONO<sub>2</sub>) and OA concentrations ( $C_{\text{OA}}$ ). Moreover, because saturation concentration is dependent on temperature, we separate the observations into a series of temperature bins and solve for fitting parameters  $f_j$  in each temperature bin, as shown in Figure 4, for both TD-LIF and CU-AMS observations. As expected, organic nitrates become less volatile at lower temperatures. At all temperatures, 10–39% of organic nitrates can be represented with  $C^* \leq 3 \mu\text{g m}^{-3}$ , meaning that they will dominantly be condensed at the average observed OA concentrations of  $\approx 9.8 \mu\text{g m}^{-3}$ . At high temperatures ( $\approx 300$  K), 73–76% of organic nitrates can be represented with  $C^* \geq 300 \mu\text{g m}^{-3}$ , meaning that they will dominantly remain in the gas phase at observed OA concentrations. At low temperatures ( $\approx 286$  K), the TD-LIF measurements suggest that 67% of organic nitrates can be represented with  $C^* \geq 300 \mu\text{g m}^{-3}$  and the CU-AMS measurements suggest that 61% of organic nitrates can be represented with  $C^* \geq 30 \mu\text{g m}^{-3}$ .

We also fit the data to eq 2 using an empirical relationship between  $C^*$  and  $\Delta H_{\text{vap}}$  from Epstein et al.<sup>84</sup> to examine the variation of RONO<sub>2</sub> volatilities observed at different temperatures but referenced to 300 K. Figure S15 shows the distribution of  $C^*$  (300 K) for RONO<sub>2</sub> during KORUS-AQ.

**3.3. CMAQ Modeling Misses a Large Source of Semivolatile, Anthropogenically Derived RONO<sub>2</sub>.** To test the efficacy of our simulations, we compare modeled and

measured NO<sub>x</sub>, O<sub>3</sub>, and O<sub>x</sub> ( $\equiv \text{O}_3 + \text{NO}_2$ ) mixing ratios at the Olympic Park ground site in Seoul, as shown in Figure S13. Our CMAQ simulation is able to capture the diurnal patterns in NO<sub>x</sub>, O<sub>3</sub>, and O<sub>x</sub> and does not show a systematic under- or over-estimation. Additionally, we compare measured and modeled OA concentrations at KIST (Korea Institute of Science and Technology, Seoul) during the campaign (see Figure S13). The CMAQ simulation is able to accurately capture the regional OA background concentration and many of the episodic events with elevated OA. Moreover, a multimodel intercomparison study of air quality simulations for the KORUS-AQ campaign used comparisons of PM<sub>1</sub> to show that models, including CMAQ, were generally able to capture the synoptic meteorological patterns during the campaign.<sup>85</sup> We also include a comparison of measured and modeled temperature on the DC-8 in Figure S13, which shows that our CMAQ simulations are able to capture the observed variability in temperature.

However, our CMAQ simulation underpredicts measured tRONO<sub>2</sub> concentrations by a factor of  $\approx 3$ , as shown by the slopes reported in Table 1 and plotted in Figure S14. Moreover, our CMAQ simulation underpredicts measured pRONO<sub>2</sub> concentrations by a factor of  $\approx 10$ , indicating that the RONO<sub>2</sub> in CMAQ are too volatile. These underpredictions for both tRONO<sub>2</sub> and pRONO<sub>2</sub> indicate that our simulation is missing a large source of condensable RONO<sub>2</sub>. We note that the RACM2\_Berkeley2.1 mechanism does not include Cl-initiated oxidation of VOCs; however, based on observations, we estimate that the production rate of RO<sub>2</sub> radicals from Cl-oxidation is an order of magnitude slower than that from OH-initiated oxidation (see Section S6) and is therefore insufficient to explain the missing source of RONO<sub>2</sub>.

To help determine the origin of the missing source of RONO<sub>2</sub>, we examine the correlation between the model-measurement RONO<sub>2</sub> difference (RONO<sub>2,diff</sub>) and measurements of various VOC classes. We find  $R^2 < 0.05$  for the correlation between RONO<sub>2,diff</sub> and both isoprene and  $\alpha$ -pinene, whereas there are relatively stronger correlations between RONO<sub>2,diff</sub> and anthropogenic alkanes ( $R^2 = 0.15$ ), alkenes ( $R^2 = 0.12$ ), aromatics ( $R^2 = 0.23$ ), and aldehydes ( $R^2 = 0.67$ ). The weak correlations between RONO<sub>2,diff</sub> and VOCs of biogenic origin and the relatively stronger correlations between RONO<sub>2,diff</sub> and VOCs of anthropogenic origin suggest that the missing source of condensable RONO<sub>2</sub> is derived from anthropogenic VOCs.

Note that the missing source of RONO<sub>2</sub> over the Korean Peninsula is likely derived from both the transport of RONO<sub>2</sub> produced in China and from locally produced RONO<sub>2</sub>. As shown in Figure 2, CMAQ underpredicts RONO<sub>2</sub> over the Yellow Sea, a region influenced by the transport of air from China during parts of the KORUS-AQ campaign, as well as over the urban centers of the Korean peninsula where local chemistry contributes to the observed RONO<sub>2</sub>.

Furthermore, the RACM2\_Berkeley2.1 mechanism was initially tested and validated on a regional scale over the Southeast United States, an area dominated by biogenic emissions.<sup>22,57</sup> Additionally, as described in Section 2.4, we adjusted the emissions of monoterpenes to improve the model-measurement agreement for biogenic VOCs. Though we expect some changes in the oxidation product distribution between low- $\text{NO}_x$  environments (e.g., Southeast United States) and high- $\text{NO}_x$  environments (e.g., Seoul), we are reasonably confident that our CMAQ simulation is accurately capturing the production and fate of  $\text{RONO}_2$  derived from biogenic VOCs. We therefore attribute the missing source of  $\text{RONO}_2$  in our simulations to  $\text{RONO}_2$  of anthropogenic origin. The previous work evaluating RACM2\_Berkeley2.1 in the Southeast United States<sup>22,57</sup> did not look at urban  $\text{RONO}_2$  in the United States, but we have no reason to suspect that this missing source of condensable  $\text{RONO}_2$  is not a general phenomenon.

The relationship between CMAQ modeled  $F_p$  ( $\text{RONO}_2$ ), OA, and temperature is shown in Figure 4c. In contrast to the observations (Figure 4a,b) and in contrast with absorptive partitioning theory, the modeled  $F_p$  increases with increasing temperature and decreases with increasing OA. Exploration of the speciated distribution of modeled  $\text{RONO}_2$  (shown in Figure S16) indicates that the increase in modeled  $F_p$  with temperature is driven largely by a temperature-dependent change in the  $\text{RONO}_2$  speciation. The phase partitioning of each  $\text{RONO}_2$  species is controlled by absorptive partitioning, meaning that the fraction of an individual  $\text{RONO}_2$  species in the particle phase increases with decreasing temperature. However, the modeled increase in the total concentration of low-volatility monoterpene nitrates (HONIT) with temperature is larger than the modeled change in concentration of other higher-volatility nitrates with temperature. As a result, the concentration of p $\text{RONO}_2$  increases with increasing temperature faster than the concentration of g $\text{RONO}_2$  increases with increasing temperature, causing the total  $F_p$  to increase with increasing temperature. This modeled relationship between  $F_p$  and temperature stands in stark disagreement with the observations and therefore indicates that the species distribution of  $\text{RONO}_2$  over Korea is incorrectly captured in our CMAQ simulation.

To test and quantify our hypothesis that our CMAQ simulation is missing a large source of condensable, anthropogenic  $\text{RONO}_2$ , we test the effect of adding an additional source of  $\text{RONO}_2$ . Because our CMAQ simulation underpredicts measured t $\text{RONO}_2$  concentrations by a factor of  $\approx 3$  (Table 1), we assign this additional source to have double the concentration of the existing simulated  $\text{RONO}_2$ . To determine the average volatility of this missing source of  $\text{RONO}_2$ , we iteratively vary its assigned  $C^*$  by an order of magnitude ( $C^* = 30, 300, \text{ and } 3000 \mu\text{g m}^{-3}$ ) and use an empirical relationship between  $C^*$  and  $\Delta H_{\text{vap}}$  from Epstein et al.<sup>84</sup> We find the best agreement between modeled and measured p $\text{RONO}_2$  and  $F_p$  with  $C^* = 300 \mu\text{g m}^{-3}$ , as shown in Table S2. Although comparison between modeled and measured  $\text{RONO}_2$  remains relatively scattered (see Figure S14) and the missing source likely includes a variety of molecules with a range of volatilities, adding this missing semivolatile  $\text{RONO}_2$  source improves the magnitude of the model-measurement agreement for t $\text{RONO}_2$ , p $\text{RONO}_2$ , and  $F_p$ , as shown in Table 1. Moreover, as shown in Figure 4, addition of this unknown source of relatively condensable

$\text{RONO}_2$  results in an increase in  $F_p$  with decreasing temperature and increasing OA concentration. This relationship between  $F_p$ , temperature, and OA is in agreement with the observations and with the equilibrium absorptive partitioning theory.

#### 4. DISCUSSION

The RACM2\_Berkeley2.1 mechanism represents our state-of-the-science understanding of  $\text{RONO}_2$  chemistry, where the only sources of semivolatile  $\text{RONO}_2$  are biogenic. However, this mechanism only captures one-third of the  $\text{RONO}_2$  production over the Korean Peninsula. Moreover, the unknown source of organic nitrates consists of  $\text{RONO}_2$  that have lower volatility than most of the existing  $\text{RONO}_2$  in the model. Consequently, our current understanding of  $\text{RONO}_2$  chemistry is missing pathways for semivolatile  $\text{RONO}_2$  production as a result of either missing oxidation pathways (first- or multi-generation, bimolecular or unimolecular) and/or an underestimation of  $\text{RONO}_2$  yields.

Because the known chemistry can only account for one-third of the observed  $\text{RONO}_2$ , the missing source is approximately double in magnitude relative to the known sources. During KORUS-AQ, the average reactivity of all measured VOCs with OH was  $2.4 \text{ s}^{-1}$ , and the effective average  $\text{RONO}_2$  yield ( $\alpha$ ), weighted by reactivity, was 1.3%. If the unknown source of  $\text{RONO}_2$  has a low  $\alpha$  of 1%, the missing reactivity must be  $\approx 3 \text{ s}^{-1}$ . On the other hand, if the unknown source of  $\text{RONO}_2$  has a higher  $\alpha$  of 20%, the missing reactivity must be  $\approx 0.15 \text{ s}^{-1}$ . For reference, during KORUS-AQ, the average isoprene reactivity was  $0.051 \text{ s}^{-1}$  and the average toluene reactivity was  $0.054 \text{ s}^{-1}$ .

We hypothesize three potential missing sources of semivolatile  $\text{RONO}_2$ : (1) missing source(s) of semi- and intermediate-volatility organic compounds (S/IVOCs) that are oxidized to  $\text{RONO}_2$ ; (2) unrepresented autoxidation mechanisms that produce highly oxygenated organic peroxy radicals ( $\text{RO}_2$ ) which could react with NO to form  $\text{RONO}_2$ ; or (3) more generations of bimolecular oxidation that are currently represented.

S/IVOCs are considered major SOA precursors, for example, refs 12, 14, 37, and 86–93, but their concentrations are challenging to measure in the atmosphere due to condensation within instruments, for example, ref 94, and their chemistry is difficult to measure in chamber experiments due to wall loss, for example, ref 95. Nault et al.<sup>37</sup> concluded that during KORUS-AQ, S/IVOCs and reactive aromatics contributed to 70% of the total SOA over Seoul. Because they are emitted with relatively low volatility, the oxidation of S/IVOCs to form  $\text{RONO}_2$  could contribute to the missing source of semivolatile  $\text{RONO}_2$ . The addition of a nitrate group decreases a molecule's volatility by  $\approx 2.2$  orders of magnitude,<sup>36</sup> meaning a missing  $\text{RONO}_2$  source with a saturation concentration of  $300 \mu\text{g m}^{-3}$  implies a precursor with  $C^* = 10^5 \mu\text{g m}^{-3}$ , namely, an IVOC. The contribution of S/IVOCs to p $\text{RONO}_2$  is not unprecedented; Lee et al.<sup>31</sup> showed that much of the p $\text{RONO}_2$  formation in the Alberta oil sands occurred via the photo-oxidation of IVOCs under high- $\text{NO}_x$  conditions.

Autoxidation, a mechanism involving an intramolecular hydrogen shift followed by the addition of molecular oxygen in  $\text{RO}_2$  radicals, can quickly (in seconds) generate highly oxygenated molecules or HOMs<sup>96,97</sup> and references therein. Because of their high oxygen content, HOMs have significantly

reduced volatility compared to their parent VOCs, for example, refs 98–100. Although autoxidation becomes relatively more competitive with bimolecular oxidation pathways as  $\text{NO}_x$  decreases, absolute rates of autoxidation increase with increasing  $\text{NO}_x$  due to increased oxidant availability.<sup>101</sup> In Korea's high- $\text{NO}_x$  environment, autoxidation may generate highly oxidized  $\text{RO}_2$  which could produce  $\text{RONO}_2$  via the reaction with NO (R2). While most previous studies of HOMs have focused on the autoxidation of  $\text{RO}_2$  derived from biogenic VOCs, theoretical calculations by Wang et al.<sup>102</sup> indicate that substituted benzenes, which were measured in high abundance during KORUS-AQ,<sup>42,63</sup> may also produce HOMs through the autoxidation of bicyclic peroxy radicals. Beginning with a substituted benzene molecule with  $C^* \approx 10^7 \mu\text{g m}^{-3}$ , one hydrogen-shift reaction resulting in the addition of a hydroperoxide group would reduce the volatility by  $\approx 2.5$  orders of magnitude, and further addition of a nitrate group would reduce the volatility by  $\approx 2.2$  orders of magnitude,<sup>36</sup> resulting in a  $C^* \approx 10^2 \mu\text{g m}^{-3}$  compound. Consequently, only one hydrogen-shift reaction is necessary to convert a substituted aromatic compound to a nitrate of the missing volatility.

Additionally, multiple recent studies have suggested that multigeneration OH oxidation of aromatics can lead to highly oxygenated oxidation products, many of which, particularly under high- $\text{NO}_x$  conditions, contain nitrogen, for example, refs 103–105. Some of these nitrogen-containing products are likely organic nitrates, but the nitrogen-containing product distribution also includes peroxy nitrates and nitro aromatics. Because aromatics are a large contributor to total VOCs over Korea,<sup>42,63</sup> there could be significant production of semivolatile, multifunctional, oxygenated organic nitrates from the multigeneration oxidation of aromatic VOCs.

In summary, exploration of the phase partitioning of  $\text{RONO}_2$  over the Korean peninsula using our aircraft-based measurements of p $\text{RONO}_2$  and t $\text{RONO}_2$  during KORUS-AQ as an example of urban chemistry indicates that organic nitrates contribute  $\approx 15\%$  of the total OA. This significant contribution of organic nitrates to the OA burden, as has been observed elsewhere, reinforces the notion that a better understanding of the processes that control the production, loss, and phase partitioning of  $\text{RONO}_2$  is crucial for understanding the processes that control SOA production and loss. Our current understanding of  $\text{RONO}_2$  chemistry can only explain one-third of the observed  $\text{RONO}_2$  in Korea and is therefore missing a source of semivolatile, anthropogenically derived  $\text{RONO}_2$  in and around Seoul. We recommend further laboratory and field research to determine the source VOCs and mechanisms that drive the production of this missing source of organic nitrates.

## ■ ASSOCIATED CONTENT

### SI Supporting Information

The Supporting Information is available free of charge at <https://pubs.acs.org/doi/10.1021/acs.est.1c05521>.

Particle loss corrections applied to TD-LIF measurements, CU-AMS measurements of p $\text{RONO}_2$ , comparison of TD-LIF and CU-AMS p $\text{RONO}_2$  measurements, CU-AMS measurements of OA, WAS measurements of VOCs, comparison of OH and Cl-oxidation of VOCs, CMAQ emissions, model-measurement comparison, and CMAQ-modeled  $\text{RONO}_2$  speciation ([PDF](#))

## ■ AUTHOR INFORMATION

### Corresponding Author

Ronald C. Cohen – Department of Chemistry, University of California, Berkeley, California 94720, United States; Department of Earth & Planetary Sciences, University of California, Berkeley CA 94720, United States; [orcid.org/0000-0001-6617-7691](https://orcid.org/0000-0001-6617-7691); Email: [rccohen@berkeley.edu](mailto:rccohen@berkeley.edu)

### Authors

Hannah S. Kenagy – Department of Chemistry, University of California, Berkeley, California 94720, United States; Present Address: Department of Chemistry, University of Michigan, Ann Arbor, Michigan 48109, United States; [orcid.org/0000-0002-0096-530X](https://orcid.org/0000-0002-0096-530X)

Paul S. Romer Present – Department of Chemistry, University of California, Berkeley, California 94720, United States; Present Address: Colorado Department of Public Health and Environment, Denver, Colorado 80246, United States; [orcid.org/0000-0002-4983-743X](https://orcid.org/0000-0002-4983-743X)

Paul J. Wooldridge – Department of Chemistry, University of California, Berkeley, California 94720, United States

Benjamin A. Nault – Department of Chemistry and Cooperative Institute for Research in Environmental Sciences, University of Colorado, Boulder, Colorado 80309, United States; Present Address: Center for Aerosol and Cloud Chemistry, Aerodyne Research, Inc., Billerica, Massachusetts 01821, United States.

Pedro Campuzano-Jost – Department of Chemistry and Cooperative Institute for Research in Environmental Sciences, University of Colorado, Boulder, Colorado 80309, United States; [orcid.org/0000-0003-3930-010X](https://orcid.org/0000-0003-3930-010X)

Douglas A. Day – Department of Chemistry and Cooperative Institute for Research in Environmental Sciences, University of Colorado, Boulder, Colorado 80309, United States; [orcid.org/0000-0003-3213-4233](https://orcid.org/0000-0003-3213-4233)

Jose L. Jimenez – Department of Chemistry and Cooperative Institute for Research in Environmental Sciences, University of Colorado, Boulder, Colorado 80309, United States

Azimeh Zare – Department of Chemistry, University of California, Berkeley, California 94710, United States

Havala O.T. Pye – Office of Research and Development, US Environmental Protection Agency, Durham, North Carolina 27709, United States; [orcid.org/0000-0002-2014-2140](https://orcid.org/0000-0002-2014-2140)

Jinhyeok Yu – School of Earth Sciences and Environmental Engineering, Gwangju Institute of Science and Technology (GIST), Gwangju 61105, Republic of Korea

Chul H. Song – School of Earth Sciences and Environmental Engineering, Gwangju Institute of Science and Technology (GIST), Gwangju 61105, Republic of Korea

Donald R. Blake – Department of Chemistry, University of California, Irvine, California 92697, United States

Jung-Hun Woo – Department of Civil and Environmental Engineering, Konkuk University, Seoul 05029, Republic of Korea

Younha Kim – Energy, Climate, and Environment (ECE) Program, International Institute for Applied Systems Analysis (IIASA), Laxenburg A-2361, Austria

Complete contact information is available at:

<https://pubs.acs.org/10.1021/acs.est.1c05521>

### Notes

The authors declare no competing financial interest.

## ACKNOWLEDGMENTS

This work was supported by NASA grant 80NSSC18K0624 and an NSF GRFP for HSK (DGE1106400). B.A.N., P.C.-J., D.A.D., and J.L.J. acknowledge NASA grant NNX15SAT96G and 80NSSC18K0630 for support. This research used the Savio computational cluster resource provided by the Berkeley Research Computing program at the University of California, Berkeley (supported by the UC Berkeley Chancellor, Vice Chancellor of Research, and Office of the CIO). We thank the Wennberg group at Caltech for the use of their second-generation isoprene nitrate measurements and the NASA Langley LARGE team for their LAS measurements. KORUS-AQ data are available at <http://doi.org/10.5067/Suborbital/KORUSAQ/DATA01>. The CMAQ model code associated with this work can be found in the Environmental Protection Agency Science Hub repository (<https://catalog.data.gov/harvest/about/epa-sciencehub>, DOI: 10.23719/1503432). RACM2\_Berkeley2.1 mechanism code can be found at [https://github.com/CohenBerkeleyLab/MECH\\_RACM](https://github.com/CohenBerkeleyLab/MECH_RACM). The US Environmental Protection Agency, through its Office of Research and Development, collaborated in the research described here. The research has been subjected to Agency administrative review and approved for publication but may not necessarily reflect official Agency policy. The views expressed in this article are those of the authors and do not necessarily represent the views or policies of the US Environmental Protection Agency.

## REFERENCES

- (1) Heald, C. L.; Jacob, D. J.; Park, R. J.; Russell, L. M.; Huebert, B. J.; Seinfeld, J. H.; Liao, H.; Weber, R. J. A large organic aerosol source in the free troposphere missing from current models. *Geophys. Res. Lett.* **2005**, *32*, L18809.
- (2) Murphy, D. M.; Cziczo, D. J.; Froyd, K. D.; Hudson, P. K.; Matthew, B. M.; Middlebrook, A. M.; Peltier, R. E.; Sullivan, A.; Thomson, D. S.; Weber, R. J. Single-particle mass spectrometry of tropospheric aerosol particles. *J. Geophys. Res.* **2006**, *111*, D23S32.
- (3) Zhang, Q.; Jimenez, J. L.; Canagaratna, M. R.; Allan, J. D.; Coe, H.; Ulbrich, I.; Alfarra, M. R.; Takami, A.; Middlebrook, A. M.; Sun, Y. L.; Dzepina, K.; Dunlea, E.; Docherty, K.; Decarlo, P. F.; Salcedo, D.; Onasch, T.; Jayne, J. T.; Miyoshi, T.; Shimono, A.; Hatakeyama, S.; Takegawa, N.; Kondo, Y.; Schneider, J.; Drewnick, F.; Cottrell, L.; Griffin, R. J.; Rautiainen, J.; Sun, J. Y.; Zhang, Y. M. Ubiquity and dominance of oxygenated species in organic aerosols in anthropogenically-influenced Northern Hemisphere midlatitudes. *Geophys. Res. Lett.* **2007**, *34*, L13801.
- (4) de Gouw, J. A.; Middlebrook, A. M.; Warneke, C.; Goldan, P. D.; Kuster, W. C.; Roberts, J. M.; Fehsenfeld, F. C.; Worsnop, D. R.; Canagaratna, M. R.; Pszenny, A. A. P.; Keene, W. C.; Marchewka, M.; Bertman, S. B.; Bates, T. S. Budget of organic carbon in a polluted atmosphere : Results from the New England Air Quality Study in 2002. *J. Geophys. Res.* **2005**, *110*, D16305.
- (5) de Gouw, J. A.; Brock, C. A.; Atlas, E. L.; Bates, T. S.; Fehsenfeld, F. C.; Goldan, P. D.; Holloway, J. S.; Kuster, W. C.; Lerner, B. M.; Matthew, B. M.; Middlebrook, A. M.; Onasch, T. B.; Peltier, R. E.; Quinn, P. K.; Senff, C. J.; Stohl, A.; Sullivan, A. P.; Trainer, M.; Warneke, C.; Weber, R. J.; Williams, E. J. Sources of particulate matter in the northeastern United States in summer: 1 . Direct emissions and secondary formation of organic matter in urban plumes. *J. Geophys. Res.* **2008**, *113*, D08301.
- (6) Goldstein, A. H.; Galbally, I. E. Known and Unexplored Organic Constituents in the Earth's Atmosphere. *Environ. Sci. Technol.* **2007**, *41*, 1514–1521.
- (7) Jimenez, J. L.; Canagaratna, M. R.; Donahue, N. M.; Prevot, A. S. H.; Zhang, Q.; Kroll, J. H.; Decarlo, P. F.; Allan, J. D.; Coe, H.; Ng, N. L.; Aiken, A. C.; Docherty, K. S.; Ulbrich, I. M.; Grieshop, A. P.; Robinson, A. L.; Duplissy, J.; Smith, J. D.; Wilson, K. R.; Lanz, V. A.; Hueglin, C.; Sun, Y. L.; Tian, J.; Laaksonen, A.; Raatikainen, T.; Rautiainen, J.; Vaattovaara, P.; Ehn, M.; Kulmala, M.; Tomlinson, J. M.; Collins, D. R.; Cubison, M. J.; Dunlea, J.; Huffman, J. A.; Onasch, T. B.; Alfarra, M. R.; Williams, P. I.; Bower, K.; Kondo, Y.; Schneider, J.; Drewnick, F.; Borrmann, S.; Weimer, S.; Demerjian, K.; Salcedo, D.; Cottrell, L.; Griffin, R.; Takami, A.; Miyoshi, T.; Hatakeyama, S.; Shimono, A.; Sun, J. Y.; Zhang, Y. M.; Dzepina, K.; Kimmel, J. R.; Sueper, D.; Jayne, J. T.; Herndon, S. C.; Trimborn, A. M.; Williams, L. R.; Wood, E. C.; Middlebrook, A. M.; Kolb, C. E.; Baltensperger, U.; Worsnop, D. R. Evolution of Organic Aerosols in the Atmosphere. *Science* **2009**, *326*, 1525–1529.
- (8) Hodzic, A.; Campuzano-Jost, P.; Bian, H.; Chin, M.; Colarco, P. R.; Day, D. A.; Froyd, K. D.; Heinold, B.; Jo, D. S.; Katich, J. M.; Kodros, J. K.; Nault, B. A.; Pierce, J. R.; Ray, E.; Schacht, J.; Schill, G. P.; Schroder, J. C.; Schwarz, J. P.; Sueper, D. T.; Tegen, I.; Tilmes, S.; Tsagiris, K.; Yu, P.; Jimenez, J. L. Characterization of organic aerosol across the global remote troposphere: A comparison of ATom measurements and global chemistry models. *Atmos. Chem. Phys.* **2020**, *20*, 4607–4635.
- (9) Volkamer, R.; Jimenez, J. L.; Martini, F. S.; Dzepina, K.; Zhang, Q.; Salcedo, D.; Molina, L. T.; Worsnop, D. R.; Molina, M. J. Secondary organic aerosol formation from anthropogenic air pollution : Rapid and higher than expected. *Geophys. Res. Lett.* **2006**, *33*, L17811.
- (10) Hallquist, M.; Wenger, J. C.; Baltensperger, U.; Rudich, Y.; Simpson, D.; Claeys, M.; Dommen, J.; Donahue, N. M.; George, C.; Goldstein, A. H.; Hamilton, J. F.; Herrmann, H.; Hoffmann, T.; Iinuma, Y.; Jang, M.; Jenkin, M. E.; Jimenez, J. L.; Kiendler-Scharr, A.; Maenhaut, W.; McFiggans, G.; Mentel, T. F.; Monod, A.; Prévôt, A. S. H.; Seinfeld, J. H.; Surratt, J. D.; Szmigielski, R.; Wildt, J. The formation , properties and impact of secondary organic aerosol : current and emerging issues. *Atmos. Chem. Phys.* **2009**, *9*, 5155–5236.
- (11) Heald, C. L.; Kroll, J. H.; Jimenez, J. L.; Docherty, K. S.; Decarlo, P. F.; Aiken, A. C.; Chen, Q.; Martin, S. T.; Farmer, D. K.; Artaxo, P. A simplified description of the evolution of organic aerosol composition in the atmosphere. *Geophys. Res. Lett.* **2010**, *37*, L08803.
- (12) Hayes, P. L.; Carlton, A. G.; Baker, K. R.; Ahmadov, R.; Washenfelder, R. A.; Alvarez, S.; Rappenglück, B.; Gilman, J. B.; Kuster, W. C.; de Gouw, J. A.; Zotter, P.; Prévôt, A. S. H.; Szidat, S.; Kleindienst, T. E.; Offenberg, J. H.; Ma, P. K.; Jimenez, J. L. Modeling the formation and aging of secondary organic aerosols in Los Angeles during CalNex 2010. *Atmos. Chem. Phys.* **2015**, *15*, 5773–5801.
- (13) Woody, M. C.; Baker, K. R.; Hayes, P. L.; Jimenez, J. L.; Koo, B.; Pye, H. O. T. Understanding sources of organic aerosol during CalNex-2010 using the CMAQ-VBS. *Atmos. Chem. Phys.* **2016**, *16*, 4081–4100.
- (14) Ma, P. K.; Zhao, Y.; Robinson, A. L.; Worton, D. R.; Goldstein, A. H.; Ortega, A. M.; Jimenez, J. L.; Zotter, P.; Prévôt, A. S. H.; Szidat, S.; Hayes, P. L. Evaluating the impact of new observational constraints on P-S/IVOC emissions, multi-generation oxidation, and chamber wall losses on SOA modeling for Los Angeles, CA. *Atmos. Chem. Phys.* **2017**, *17*, 9237–9259.
- (15) Shrivastava, M.; Cappa, C. D.; Fan, J.; Goldstein, A. H.; Guenther, A. B.; Jimenez, J. L.; Kuang, C.; Laskin, A.; Martin, S. T.; Ng, N. L.; Petaja, T.; Pierce, J. R.; Rasch, P. J.; Roldin, P.; Seinfeld, J. H.; Shilling, J.; Smith, J. N.; Thornton, J. A.; Volkamer, R.; Wang, J.; Worsnop, D. R.; Zaveri, R. A.; Zelenyuk, A.; Zhang, Q. Recent advances in understanding secondary organic aerosol: Implications for global climate forcing. *Rev. Geophys.* **2017**, *55*, 509–559.
- (16) Tsimpidi, A. P.; Karydis, V. A.; Pandis, S. N.; Lelieveld, J. Global-scale combustion sources of organic aerosols : sensitivity to formation and removal mechanisms. *Atmos. Chem. Phys.* **2017**, *17*, 7345–7364.
- (17) Ayres, B. R.; Allen, H. M.; Draper, D. C.; Brown, S. S.; Wild, R. J.; Jimenez, J. L.; Day, D. A.; Campuzano-Jost, P.; Hu, W.; De Gouw, J.; Koss, A.; Cohen, R. C.; Duffey, K. C.; Romer, P.; Baumann, K.; Edgerton, E.; Takahama, S.; Thornton, J. A.; Lee, B. H.; Lopez-Hilfiker, F. D.; Mohr, C.; Wennberg, P. O.; Nguyen, T. B.; Teng, A.;

- Goldstein, A. H.; Olson, K.; Fry, J. L. Organic nitrate aerosol formation via NO<sub>3</sub> + biogenic volatile organic compounds in the southeastern United States. *Atmos. Chem. Phys.* **2015**, *15*, 13377–13392.
- (18) Pye, H. O. T.; Luecken, D. J.; Xu, L.; Boyd, C. M.; Ng, N. L.; Baker, K. R.; Ayres, B. R.; Bash, J. O.; Baumann, K.; Carter, W. P. L.; Edgerton, E.; Fry, J. L.; Hutzell, W. T.; Schwede, D. B.; Shepson, P. B. Modeling the Current and Future Roles of Particulate Organic Nitrates in the Southeastern United States. *Environ. Sci. Technol.* **2015**, *49*, 14195–14203.
- (19) Xu, L.; Guo, H.; Boyd, C. M.; Klein, M.; Bougiatioti, A.; Cerully, K. M.; Hite, J. R.; Isaacman-VanWertz, G.; Kreisberg, N. M.; Knote, C.; Olson, K.; Koss, A.; Goldstein, A. H.; Hering, S. V.; De Gouw, J.; Baumann, K.; Lee, S.-H.; Nenes, A.; Weber, R. J.; Ng, N. L. Effects of anthropogenic emissions on aerosol formation from isoprene and monoterpenes in the southeastern United States. *Proc. Natl. Acad. Sci. U.S.A.* **2015**, *112*, 37–42.
- (20) Fisher, J. A.; Jacob, D. J.; Travis, K. R.; Kim, P. S.; Marais, E. A.; Chan Miller, C.; Yu, K.; Zhu, L.; Yantosca, R. M.; Sulprizio, M. P.; Mao, J.; Wennberg, P. O.; Crounse, J. D.; Teng, A. P.; Nguyen, T. B.; St. Clair, J. M.; Cohen, R. C.; Romer, P.; Nault, B. A.; Wooldridge, P. J.; Jimenez, J. L.; Campuzano-Jost, P.; Day, D. A.; Hu, W.; Shepson, P. B.; Xiong, F.; Blake, D. R.; Goldstein, A. H.; Misztal, P. K.; Hanisco, T. F.; Wolfe, G. M.; Ryerson, T. B.; Wisthaler, A.; Mikoviny, T. Organic nitrate chemistry and its implications for nitrogen budgets in an isoprene- and monoterpene-rich atmosphere : constraints from aircraft (SEAC\$4\$RS) and ground-based (SOAS) observations in the Southeast US. *Atmos. Chem. Phys.* **2016**, *16*, 5969–5991.
- (21) Lee, B. H.; Mohr, C.; Lopez-Hilfiker, F. D.; Lutz, A.; Hallquist, M.; Lee, L.; Romer, P.; Cohen, R. C.; Iyer, S.; Kurtén, T.; Hu, W.; Day, D. A.; Campuzano-Jost, P.; Jimenez, J. L.; Xu, L.; Ng, N. L.; Guo, H.; Weber, R. J.; Wild, R. J.; Brown, S. S.; Koss, A.; de Gouw, J.; Olson, K.; Goldstein, A. H.; Seco, R.; Kim, S.; McAvey, K.; Shepson, P. B.; Starn, T.; Baumann, K.; Edgerton, E. S.; Liu, J.; Shilling, J. E.; Miller, D. O.; Brune, W.; Schobesberger, S.; D'Ambro, E. L.; Thornton, J. A. Highly functionalized organic nitrates in the southeast United States: Contribution to secondary organic aerosol and reactive nitrogen budgets. *Proc. Natl. Acad. Sci. U.S.A.* **2016**, *113*, 1516–1521.
- (22) Zare, A.; Fahey, K. M.; Sarwar, G.; Cohen, R. C.; Pye, H. O. T. Vapor-Pressure Pathways Initiate but Hydrolysis Products Dominate the Aerosol Estimated from Organic Nitrates. *ACS Earth Space Chem.* **2019**, *3*, 1426–1437.
- (23) Fry, J. L.; Draper, D. C.; Zarzana, K. J.; Campuzano-Jost, P.; Day, D. A.; Jimenez, J. L.; Brown, S. S.; Cohen, R. C.; Kaser, L.; Hansel, A.; Cappellin, L.; Karl, T.; Hodzic Roux, A.; Turnipseed, A.; Cantrell, C.; Lefer, B. L.; Grossberg, N. Observations of gas- and aerosol-phase organic nitrates at BEACHON-RoMBAS 2011. *Atmos. Chem. Phys.* **2013**, *13*, 8585–8605.
- (24) Kiendler-Scharr, A.; Mensah, A. A.; Friese, E.; Topping, D.; Nemitz, E.; Prevot, A. S.; Äijälä, M.; Allan, J.; Canonaco, F.; Canagaratna, M.; Carbone, S.; Crippa, M.; Dall Osto, M.; Day, D. A.; De Carlo, P.; Di Marco, C. F.; Elbern, H.; Eriksson, A.; Freney, E.; Hao, L.; Herrmann, H.; Hildebrandt, L.; Hillamo, R.; Jimenez, J. L.; Laaksonen, A.; McFiggans, G.; Mohr, C.; O'Dowd, C.; Otjes, R.; Ovadnevaite, J.; Pandis, S. N.; Poulain, L.; Schlag, P.; Sellegri, K.; Swietlicki, E.; Tiitta, P.; Vermeulen, A.; Wahner, A.; Worsnop, D.; Wu, H. C. Ubiquity of organic nitrates from nighttime chemistry in the European submicron aerosol. *Geophys. Res. Lett.* **2016**, *43*, 7735–7744.
- (25) Hao, L. Q.; Kortelainen, A.; Romakkaniemi, S.; Portin, H.; Jaatinen, A.; Leskinen, A.; Komppula, M.; Miettinen, P.; Sueper, D.; Pajunoja, A.; Smith, J. N.; Lehtinen, K. E. J.; Worsnop, D. R.; Laaksonen, A.; Virtanen, A. Atmospheric submicron aerosol composition and particulate organic nitrate formation in a boreal forestland-urban mixed region. *Atmos. Chem. Phys.* **2014**, *14*, 13483–13495.
- (26) Rollins, A. W.; Browne, E. C.; Min, K.-E.; Pusede, S. E.; Wooldridge, P. J.; Gentner, D. R.; Goldstein, A. H.; Liu, S.; Day, D.; Russell, L. M.; Cohen, R. C. Evidence for NO<sub>x</sub> Control over Nighttime SOA Formation. *Science* **2012**, *337*, 1210–1212.
- (27) Rollins, A. W.; Pusede, S.; Wooldridge, P.; Min, K.-E.; Gentner, D. R.; Goldstein, A. H.; Liu, S.; Day, D. A.; Russell, L. M.; Rubitschun, C. L.; Surratt, J. D.; Cohen, R. C. Gas-particle partitioning of total alkyl nitrates observed with TD-LIF in Bakersfield. *J. Geophys. Res. Atmos.* **2013**, *118*, 6651–6662.
- (28) Zhu, Q.; He, L.-Y.; Huang, X.-F.; Cao, L.-M.; Gong, Z.-H.; Wang, C.; Zhuang, X.; Hu, M. Atmospheric aerosol compositions and sources at two national background sites in northern and southern China. *Atmos. Chem. Phys.* **2016**, *16*, 10283–10297.
- (29) Xu, W.; Takeuchi, M.; Chen, C.; Qiu, Y.; Xie, C.; Xu, W.; Ma, N.; Worsnop, D.; Ng, N. L.; Sun, Y. Estimation of particulate organic nitrates from thermodenuder-aerosol mass spectrometer measurements in North China Plain. *Atmos. Meas. Tech. Discuss.* **2021**, *14*, 3693–3705.
- (30) Zhu, Q.; Cao, L.-M.; Tang, M.-X.; Huang, X.-F.; Saikawa, E.; He, L.-Y. Characterization of Organic Aerosol at a Rural Site in the North China Plain Region: Sources, Volatility and Organonitrates. *Adv. Atmos. Sci.* **2021**, *38*, 1115–1127.
- (31) Lee, A. K. Y.; Adam, M. G.; Liggio, J.; Li, S.-M.; Li, K.; Willis, M. D.; Abbatt, J. P. D.; Tokarek, T. W.; Odame-Ankrah, C. A.; Ostroff, H. D.; Strawbridge, K.; Brook, J. R. A Large Contribution of Anthropogenic Organo-Nitrates to Secondary Organic Aerosol in the Alberta Oil Sands. *Atmos. Chem. Phys.* **2019**, *19*, 12209–12219.
- (32) Lee, L.; Wooldridge, P. J.; DeGouw, J.; Brown, S. S.; Bates, T. S.; Quinn, P. K.; Cohen, R. C. Particulate organic nitrates observed in an oil and natural gas production region during wintertime. *Atmos. Chem. Phys.* **2015**, *15*, 9313–9325.
- (33) Zhang, J. K.; Cheng, M. T.; Ji, D. S.; Liu, Z. R.; Hu, B.; Sun, Y.; Wang, Y. S. Characterization of submicron particles during biomass burning and coal combustion periods in Beijing, China. *Sci. Total Environ.* **2016**, *562*, 812–821.
- (34) Yu, K.; Zhu, Q.; Du, K.; Huang, X.-F. Characterization of nighttime formation of particulate organic nitrates based on high-resolution aerosol mass spectrometry in an urban atmosphere in China. *Atmos. Chem. Phys.* **2019**, *19*, 5235–5249.
- (35) Fry, J. L.; Brown, S. S.; Middlebrook, A. M.; Edwards, P. M.; Campuzano-Jost, P.; Day, D. A.; Jimenez, J. L.; Allen, H. M.; Ryerson, T. B.; Pollack, I.; Graus, M.; Warneke, C.; De Gouw, J. A.; Brock, C. A.; Gilman, J.; Lerner, B. M.; Dubé, W. P.; Liao, J.; Welti, A. Secondary organic aerosol (SOA) yields from NO<sub>3</sub> radical + isoprene based on nighttime aircraft power plant plume transects. *Atmos. Chem. Phys.* **2018**, *18*, 11663–11682.
- (36) Pankow, J. F.; Asher, W. E. SIMPOL.1: A simple group contribution method for predicting vapor pressures and enthalpies of vaporization of multifunctional organic compounds. *Atmos. Chem. Phys.* **2008**, *8*, 2773–2796.
- (37) Nault, B. A.; Campuzano-Jost, P.; Day, D. A.; Schroder, J. C.; Anderson, B.; Beyersdorf, A. J.; Blake, D. R.; Brune, W. H.; Choi, Y.; Corr, C. A.; de Gouw, J. A.; Dibb, J.; DiGangi, J. P.; Diskin, G. S.; Fried, A.; Huey, L. G.; Kim, M. J.; Knote, C. J.; Lamb, K. D.; Lee, T.; Park, T.; Pusede, S. E.; Scheuer, E.; Thornhill, K. L.; Woo, J.-H.; Jimenez, J. L. Secondary organic aerosol production from local emissions dominates the organic aerosol budget over Seoul, South Korea, during KORUS-AQ. *Atmos. Chem. Phys.* **2018**, *18*, 17769–17800.
- (38) Jordan, C. E.; Crawford, J. H.; Beyersdorf, A. J.; Eck, T. F.; Halliday, H. S.; Nault, B. A.; Chang, L.-S.; Park, J.; Park, R.; Lee, G.; Kim, H.; Ahn, J.-Y.; Cho, S.; Shin, H. J.; Lee, J. H.; Jung, J.; Kim, D.-S.; Lee, M.; Lee, T.; Whitehill, A.; Szykman, J.; Schueneman, M. K.; Campuzano-Jost, P.; Jimenez, J. L.; DiGangi, J. P.; Diskin, G. S.; Anderson, B. E.; Moore, R. H.; Ziembka, L. D.; Fenn, M. A.; Hair, J. W.; Kuehn, R. E.; Holz, R. E.; Chen, G.; Travis, K.; Shook, M.; Peterson, D. A.; Lamb, K. D.; Schwarz, J. P. Investigation of factors controlling PM<sub>2.5</sub> variability across the South Korean Peninsula during KORUS-AQ. *Elementa: Science of the Anthropocene* **2020**, *8*, 28.
- (39) Crawford, J. H.; Ahn, J.-Y.; Al-Saadi, J.; Chang, L.; Emmons, L. K.; Kim, J.; Lee, G.; Park, J.-H.; Park, R. J.; Woo, J. H.; Song, C.-K.

- Hong, J.-H.; Hong, Y.-D.; Lefer, B. L.; Lee, M.; Lee, T.; Kim, S.; Min, K.-E.; Yum, S. S.; Shin, H. J.; Kim, Y.-W.; Choi, J.-S.; Park, J.-S.; Szykman, J. J.; Long, R. W.; Jordan, C. E.; Simpson, I. J.; Fried, A.; Dibb, J. E.; Cho, S.; Kim, Y. P. The Korea-United States Air Quality (KORUS-AQ) field study. *Elementa: Science of the Anthropocene* **2021**, *9*, 00163.
- (40) Park, M.-s.; Park, S.-h.; Chae, J.-h.; Choi, M.-h.; Song, Y.; Kang, M.; Roh, J.-W. High-resolution urban observation network for user-specific meteorological information service in the Seoul Metropolitan Area, South Korea. *Atmos. Meas. Tech.* **2017**, *10*, 1575–1594.
- (41) Kim, H. C.; Kim, E.; Bae, C.; Cho, J. H.; Kim, B.-u.; Kim, S. Regional contributions to particulate matter concentration in the Seoul metropolitan area, South Korea: seasonal variation and sensitivity to meteorology and emissions inventory. *Atmos. Chem. Phys.* **2017**, *17*, 10315–10332.
- (42) Fried, A.; Walega, J.; Weibring, P.; Richter, D.; Simpson, I. J.; Blake, D. R.; Blake, N. J.; Meinardi, S.; Barletta, B.; Hughes, S. C.; Crawford, J. H.; Diskin, G.; Barrick, J.; Hair, J.; Fenn, M.; Wisthaler, A.; Mikoviny, T.; Woo, J.-H.; Park, M.; Kim, J.; Min, K.-E.; Jeong, S.; Wennberg, P. O.; Kim, M. J.; Crounse, J. D.; Teng, A. P.; Bennett, R.; Yang-Martin, M.; Shook, M. A.; Huey, G.; Tanner, D.; Knot, C.; Kim, J.; Park, R.; Brune, W. Airborne formaldehyde and volatile organic compound measurements over the Daesan petrochemical complex on Korea's northwest coast during the Korea-United States Air Quality study. *Elementa: Science of the Anthropocene* **2020**, *8*, 121.
- (43) Lee, B. H.; Lopez-Hilfiker, F. D.; Mohr, C.; Kurtén, T.; Worsnop, D. R.; Thornton, J. A. An iodide-adduct high-resolution time-of-flight chemical-ionization mass spectrometer: Application to atmospheric inorganic and organic compounds. *Environ. Sci. Technol.* **2014**, *48*, 6309–6317.
- (44) Shi, X.; Qiu, X.; Cheng, Z.; Chen, Q.; Rudich, Y.; Zhu, T. Isomeric Identification of Particle-Phase Organic Nitrates through Gas Chromatography and Time-of-Flight Mass Spectrometry Coupled with an Electron Capture Negative Ionization Source. *Environ. Sci. Technol.* **2020**, *54*, 707–713.
- (45) Day, D. A.; Wooldridge, P. J.; Dillon, M. B.; Thornton, J. A.; Cohen, R. C. A thermal dissociation laser-induced fluorescence instrument for in situ detection of NO<sub>2</sub>, peroxy nitrates, alkyl nitrates, and HNO<sub>3</sub>. *J. Geophys. Res. Atmos.* **2002**, *107*, 4–1.
- (46) Wooldridge, P. J.; Perring, A. E.; Bertram, T. H.; Flocke, F. M.; Roberts, J. M.; Singh, H. B.; Huey, L. G.; Thornton, J. A.; Wolfe, G. M.; Murphy, J. G.; Fry, J. L.; Rollins, A. W.; Lafranchi, B. W.; Cohen, R. C. Total Peroxy Nitrates ( $\Sigma$ PNs) in the atmosphere: The Thermal Dissociation-Laser Induced Fluorescence (TD-LIF) technique and comparisons to speciated PAN measurements. *Atmos. Meas. Tech.* **2010**, *3*, 593–607.
- (47) Rollins, A. W.; Smith, J. D.; Wilson, K. R.; Cohen, R. C. Real time in situ detection of organic nitrates in atmospheric aerosols. *Environ. Sci. Technol.* **2010**, *44*, 5540–5545.
- (48) Womack, C. C.; Neuman, J. A.; Veres, P. R.; Eilerman, S. J.; Brock, C. A.; Decker, Z. C. J.; Zarzana, K. J.; Dube, W. P.; Wild, R. J.; Wooldridge, P. J.; Cohen, R. C.; Brown, S. S. Evaluation of the accuracy of thermal dissociation CRDS and LIF techniques for atmospheric measurement of reactive nitrogen species. *Atmos. Chem. Phys.* **2017**, *10*, 1911–1926.
- (49) Friedrich, N.; Tadic, I.; Schuladen, J.; Brooks, J.; Darbyshire, E.; Drewnick, F.; Fischer, H.; Lelieveld, J.; Crowley, J. N.; Crowley, J. N. Measurement of NOx and NOy with a thermal dissociation cavity ring-down spectrometer (TD-CRDS): Instrument characterisation and first deployment. *Atmos. Meas. Tech.* **2020**, *13*, 5739–5761.
- (50) Wiedensohler, A. An approximation of the bipolar charge distribution for particles in the submicron size range. *J. Aerosol Sci.* **1988**, *19*, 387–389.
- (51) DeCarlo, P. F.; Kimmel, J. R.; Trimborn, A.; Northway, M. J.; Jayne, J. T.; Aiken, A. C.; Gonin, M.; Fuhrer, K.; Horvath, T.; Docherty, K. S.; Worsnop, D. R.; Jimenez, J. L. Field-deployable, high-resolution, time-of-flight aerosol mass spectrometer. *Anal. Chem.* **2006**, *78*, 8281–8289.
- (52) Canagaratna, M. R.; Jayne, J. T.; Jimenez, J. L.; Allan, J. D.; Alfarra, M. R.; Zhang, Q.; Onasch, T. B.; Drewnick, F.; Coe, H.; Middlebrook, A.; Delia, A.; Williams, L. R.; Trimborn, A. M.; Northway, M. J.; DeCarlo, P. F.; Kolb, C. E.; Davidovits, P.; Worsnop, D. R. Chemical and Microphysical Characterization of Ambient Aerosols with the Aerodyne Aerosol Mass Spectrometer. *Mass Spectrom. Rev.* **2007**, *26*, 185–222.
- (53) Farmer, D. K.; Matsunaga, A.; Docherty, K. S.; Surratt, J. D.; Seinfeld, J. H.; Ziemann, P. J.; Jimenez, J. L. Response of an aerosol mass spectrometer to organonitrates and organosulfates and implications for atmospheric chemistry. *Proc. Natl. Acad. Sci. U.S.A.* **2010**, *107*, 6670–6675.
- (54) Xu, L.; Suresh, S.; Guo, H.; Weber, R. J.; Ng, N. L. Aerosol characterization over the southeastern United States using high-resolution aerosol mass spectrometry: Spatial and seasonal variation of aerosol composition and sources with a focus on organic nitrates. *Atmos. Chem. Phys.* **2015**, *15*, 7307–7336.
- (55) Wyat Appel, K.; Napelenok, S.; Hogrefe, C.; Pouliot, G.; Foley, K. M.; Roselle, S. J.; Pleim, J. E.; Bash, J.; Pye, H. O. T.; Heath, N.; Murphy, B.; Mathur, R. *Overview and Evaluation of the Community Multiscale Air Quality (CMAQ) Modeling System Version 5.2*; Springer Proceedings in Complexity, 2018; pp 69–73.
- (56) Kelly, J. T.; Koplitz, S. N.; Baker, K. R.; Holder, A. L.; Pye, H. O. T.; Murphy, B. N.; Bash, J. O.; Henderson, B. H.; Possiel, N. C.; Simon, H.; Eyth, A. M.; Jang, C.; Phillips, S.; Timin, B. Assessing PM<sub>2.5</sub> model performance for the conterminous U.S. with comparison to model performance statistics from 2007–2015. *Atmos. Environ.* **2019**, *214*, 116872.
- (57) Zare, A.; Romer, P. S.; Nguyen, T.; Keutsch, F. N.; Skog, K.; Cohen, R. C. A comprehensive organic nitrate chemistry: Insights into the lifetime of atmospheric organic nitrates. *Atmos. Chem. Phys.* **2018**, *18*, 15419–15436.
- (58) Otte, T. L.; Pleim, J. E. The Meteorology-Chemistry Interface Processor (MCIP) for the CMAQ modeling system: Updates through MCIPv3.4.1. *Geosci. Model Dev.* **2010**, *3*, 243–256.
- (59) Woo, J.-H.; Kim, Y.; Kim, H. K.; Choi, K. C.; Eum, J. H.; Lee, J. B.; Lim, J. H.; Kim, J.; Seong, M. Development of the CREATE inventory in support of integrated climate and air quality modeling for Asia. *Sustainability* **2020**, *12*, 7930.
- (60) Guenther, A. B.; Jiang, X.; Heald, C. L.; Sakulyanontvittaya, T.; Duhl, T.; Emmons, L. K.; Wang, X. Model Development The Model of Emissions of Gases and Aerosols from Nature version 2.1 (MEGAN2. 1): an extended and updated framework for modeling biogenic emissions. *Geosci. Model Dev.* **2012**, *5*, 1471–1492.
- (61) Wiedinmyer, C.; Akagi, S. K.; Yokelson, R. J.; Emmons, L. K.; Al-Saadi, J. A.; Orlando, J. J.; Soja, A. J. Model Development The Fire INventory from NCAR (FINN): a high resolution global model to estimate the emissions from open burning. *Geosci. Model Dev.* **2011**, *4*, 625–641.
- (62) Houyoux, M. R.; Vukovich, J. M.; Coats, C. J.; Wheeler, N. J. M.; Kasibhatla, P. S. Emission inventory development and processing for the Seasonal Model for Regional Air Quality (SMRAQ) project. *J. Geophys. Res. Atmos.* **2000**, *105*, 9079–9090.
- (63) Simpson, I. J.; Blake, D. R.; Blake, N. J.; Meinardi, S.; Barletta, B.; Hughes, S. C.; Fleming, L. T.; Crawford, J. H.; Diskin, G. S.; Emmons, L. K.; Fried, A.; Guo, H.; Peterson, D. A.; Wisthaler, A.; Woo, J.-H.; Barré, J.; Gaubert, B.; Kim, J.; Kim, M. J.; Kim, Y.; Knot, C.; Mikoviny, T.; Pusede, S. E.; Schroeder, J. R.; Wang, Y.; Wennberg, P. O.; Zeng, L. Characterization, sources and reactivity of volatile organic compounds (VOCs) in Seoul and surrounding regions during KORUS-AQ. *Elementa: Science of the Anthropocene* **2020**, *8*, 37.
- (64) McDonald, B. C.; De Gouw, J. A.; Gilman, J. B.; Jathar, S. H.; Akherati, A.; Cappa, C. D.; Jimenez, J. L.; Lee-Taylor, J.; Hayes, P. L.; McKeen, S. A.; Cui, Y. Y.; Kim, S.-W.; Gentner, D. R.; Isaacman-VanWertz, G.; Goldstein, A. H.; Harley, R. A.; Frost, G. J.; Roberts, J. M.; Ryerson, T. B.; Trainer, M. Volatile chemical products emerging as largest petrochemical source of urban organic emissions. *Science* **2018**, *359*, 760–764.

- (65) Gkatzelis, G. I.; Coggon, M. M.; McDonald, B. C.; Peischl, J.; Aikin, K. C.; Gilman, J. B.; Trainer, M.; Warneke, C. Identifying Volatile Chemical Product Tracer Compounds in U.S. Cities. *Environ. Sci. Technol.* **2021**, *55*, 188–199.
- (66) Crounse, J. D.; McKinney, K. A.; Kwan, A. J.; Wennberg, P. O. Measurement of gas-phase hydroperoxides by chemical ionization mass spectrometry. *Anal. Chem.* **2006**, *78*, 6726–6732.
- (67) Goliff, W. S.; Stockwell, W. R.; Lawson, C. V. The regional atmospheric chemistry mechanism, version 2. *Atmos. Environ.* **2013**, *68*, 174–185.
- (68) Sarwar, G.; Godowitch, J.; Henderson, B. H.; Fahey, K.; Pouliot, G.; Hutzell, W. T.; Mathur, R.; Kang, D.; Goliff, W. S.; Stockwell, W. R. A comparison of atmospheric composition using the Carbon Bond and Regional Atmospheric Chemistry Mechanisms. *Atmos. Chem. Phys.* **2013**, *13*, 9695–9712.
- (69) Browne, E. C.; Wooldridge, P. J.; Min, K.-E.; Cohen, R. C. On the role of monoterpene chemistry in the remote continental boundary layer. *Atmos. Chem. Phys.* **2014**, *14*, 1225–1238.
- (70) Carter, W. P. L.; Atkinson, R. Alkyl Nitrate Formation from the Atmospheric Photooxidation of Alkanes; a Revised Estimation Method. *J. Atmos. Chem.* **1989**, *8*, 165–173.
- (71) Middleton, P.; Stockwell, W. R.; Carter, W. P. L. Aggregation and analysis of volatile organic compound emissions for regional modeling. *Atmos. Environ., Part A* **1990**, *24*, 1107–1133.
- (72) Arey, J.; Aschmann, S. M.; Kwok, E. S. C.; Atkinson, R. Alkyl Nitrate, Hydroxyalkyl Nitrate, and Hydroxycarbonyl Formation from the NO<sub>x</sub> - Air Photooxidations of C5-C8 w-Alkanes. *J. Phys. Chem. A* **2001**, *105*, 1020–1027.
- (73) Jenkin, M. E.; Saunders, S. M.; Pilling, M. J. The tropospheric degradation of volatile organic compounds: a protocol for mechanism development. *Atmos. Environ.* **1997**, *31*, 81–104.
- (74) Saunders, S. M.; Jenkin, M. E.; Derwent, R. G.; Pilling, M. J. Protocol for the development of the Master Chemical Mechanism, MCM v3 (Part A): tropospheric degradation of non-aromatic volatile organic compounds. *Atmos. Chem. Phys.* **2003**, *3*, 161–180.
- (75) Leungsakul, S.; Jeffries, H. E.; Kamens, R. M. A kinetic mechanism for predicting secondary aerosol formation from the reactions of d-limonene in the presence of oxides of nitrogen and natural sunlight. *Atmos. Environ.* **2005**, *39*, 7063–7082.
- (76) Spittler, M.; Barnes, I.; Bejan, I.; Brockmann, K. J.; Benter, T.; Wirtz, K. Reactions of NO<sub>3</sub> radicals with limonene and  $\alpha$ -pinene: Product and SOA formation. *Atmos. Environ.* **2006**, *40*, 116–127.
- (77) Paulot, F.; Crounse, J. D.; Kjaergaard, H. G.; Kroll, J. H.; Seinfeld, J. H.; Wennberg, P. O. Isoprene photooxidation: new insights into the production of acids and organic nitrates. *Atmos. Chem. Phys.* **2009**, *9*, 1479–1501.
- (78) Paulot, F.; Crounse, J. D.; Kjaergaard, H. G.; Kürten, A.; St. Clair, J. M.; Seinfeld, J. H.; Wennberg, P. O. Unexpected Epoxide Formation in the Gas-Phase Photooxidation of Isoprene. *Science* **2009**, *325*, 730–733.
- (79) Crounse, J. D.; Paulot, F.; Kjaergaard, H. G.; Wennberg, P. O. Peroxy radical isomerization in the oxidation of isoprene. *Phys. Chem. Chem. Phys.* **2011**, *13*, 13607–13613.
- (80) Ng, N. L.; Brown, S. S.; Archibald, A. T.; Atlas, E.; Cohen, R. C.; Crowley, J. N.; Day, D. A.; Donahue, N. M.; Fry, J. L.; Fuchs, H.; Griffin, R. J.; Guzman, M. I.; Herrmann, H.; Hodzic, A.; Iinuma, Y.; Jimenez, J. L.; Kiendler-Scharr, A.; Lee, B. H.; Luecken, D. J.; Mao, J.; McLaren, R.; Mutzel, A.; Osthoff, H. D.; Ouyang, B.; Picquet-Varrault, B.; Platt, U.; Pye, H. O. T.; Rudich, Y.; Schwantes, R. H.; Shiraiwa, M.; Stutz, J.; Thornton, J. A.; Tilgner, A.; Williams, B. J.; Zaveri, R. A. Nitrate radicals and biogenic volatile organic compounds: Oxidation, mechanisms, and organic aerosol. *Atmos. Chem. Phys.* **2017**, *17*, 2103–2162.
- (81) Xu, Z. N.; Nie, W.; Chi, X. G.; Sun, P.; Huang, D. D.; Yan, C.; Krechmer, J.; Ye, P. L.; Xu, Z.; Qi, X. M.; Zhu, C.; Liu, Y. L.; Li, Y. Y.; Wang, T. Y.; Wang, L.; Huang, X.; Tang, R. Z.; Guo, S.; Xiu, G. L.; Fu, Q. Y.; Worsnop, D.; Ding, A. J. Multifunctional products of isoprene oxidation in polluted atmosphere and their contribution to SOA. *Geophys. Res. Lett.* **2020**, *48*, No. e2020GL089276.
- (82) Donahue, N. M.; Robinson, A. L.; Stanier, C. O.; Pandis, S. N. Coupled partitioning, dilution, and chemical aging of semivolatile organics. *Environ. Sci. Technol.* **2006**, *40*, 2635–2643.
- (83) Pankow, J. F. An absorption model of the gas/aerosol partitioning involved in the formation of secondary organic aerosol. *Atmos. Environ.* **1994**, *28*, 189–193.
- (84) Epstein, S. A.; Riipinen, I.; Donahue, N. M. A semiempirical correlation between enthalpy of vaporization and saturation concentration for organic aerosol. *Environ. Sci. Technol.* **2010**, *44*, 743–748.
- (85) Park, R. J.; Oak, Y. J.; Emmons, L. K.; Kim, C. H.; Pfister, G. G.; Carmichael, G. R.; Saide, P. E.; Cho, S. Y.; Kim, S.; Woo, J. H.; Crawford, J. H.; Gaubert, B.; Lee, H. J.; Park, S. Y.; Jo, Y. J.; Gao, M.; Tang, B.; Stanier, C. O.; Shin, S. S.; Park, H. Y.; Bae, C.; Kim, E. Multi-model intercomparisons of air quality simulations for the KORUS-AQ campaign. *Elementa* **2021**, *9*, 00139.
- (86) Robinson, A. L.; Donahue, N. M.; Shrivastava, M. K.; Weitkamp, E. A.; Sage, A. M.; Grieshop, A. P.; Lane, T. E.; Pierce, J. R.; Pandis, S. N. Rethinking organic aerosols: Semivolatile emissions and photochemical aging. *Science* **2007**, *315*, 1259–1262.
- (87) Grieshop, A. P.; Logue, J. M.; Donahue, N. M.; Robinson, A. L. Laboratory investigation of photochemical oxidation of organic aerosol from wood fires 1: Measurement and simulation of organic aerosol evolution. *Atmos. Chem. Phys.* **2009**, *9*, 1263–1277.
- (88) Dzepina, K.; Volkamer, R. M.; Madronich, S.; Tulet, P.; Ulbrich, I. M.; Zhang, Q.; Cappa, C. D.; Ziemann, P. J.; Jimenez, J. L. Evaluation of recently-proposed secondary organic aerosol models for a case study in Mexico City. *Atmos. Chem. Phys.* **2009**, *9*, 5681–5709.
- (89) Hodzic, A.; Jimenez, J. L.; Madronich, S.; Canagaratna, M. R.; Decarlo, P. F.; Kleinman, L.; Fast, J. Modeling organic aerosols in a megacity: Potential contribution of semi-volatile and intermediate volatility primary organic compounds to secondary organic aerosol formation. *Atmos. Chem. Phys.* **2010**, *10*, 5491–5514.
- (90) Pye, H. O. T.; Seinfeld, J. H. A global perspective on aerosol from low-volatility organic compounds. *Atmos. Chem. Phys.* **2010**, *10*, 4377–4401.
- (91) Dzepina, K.; Cappa, C. D.; Volkamer, R. M.; Madronich, S.; Decarlo, P. F.; Zaveri, R. A.; Jimenez, J. L. Modeling the multiday evolution and aging of secondary organic aerosol during MILAGRO 2006. *Environ. Sci. Technol.* **2011**, *45*, 3496–3503.
- (92) Zhao, Y.; Hennigan, C. J.; May, A. A.; Tkacik, D. S.; De Gouw, J. A.; Gilman, J. B.; Kuster, W. C.; Borbon, A.; Robinson, A. L. Intermediate-volatility organic compounds: A large source of secondary organic aerosol. *Environ. Sci. Technol.* **2014**, *48*, 13743–13750.
- (93) Ortega, A. M.; Hayes, P. L.; Peng, Z.; Palm, B. B.; Hu, W.; Day, D. A.; Li, R.; Cubison, M. J.; Brune, W. H.; Graus, M.; Warneke, C.; Gilman, J. B.; Kuster, W. C.; De Gouw, J.; Gutiérrez-Montes, C.; Jimenez, J. L. Real-time measurements of secondary organic aerosol formation and aging from ambient air in an oxidation flow reactor in the Los Angeles area. *Atmos. Chem. Phys.* **2016**, *16*, 7411–7433.
- (94) Pagonis, D.; Krechmer, J. E.; De Gouw, J.; Jimenez, J. L.; Ziemann, P. J. Effects of gas-wall partitioning in Teflon tubing and instrumentation on time-resolved measurements of gas-phase organic compounds. *Atmos. Meas. Tech.* **2017**, *10*, 4687–4696.
- (95) Zhang, X.; Cappa, C. D.; Jathar, S. H.; McVay, R. C.; Ensberg, J. J.; Kleeman, M. J.; Seinfeld, J. H. Influence of vapor wall loss in laboratory chambers on yields of secondary organic aerosol. *Proc. Natl. Acad. Sci. U.S.A.* **2014**, *111*, S802–S807.
- (96) Crounse, J. D.; Nielsen, L. B.; Jørgensen, S.; Kjaergaard, H. G.; Wennberg, P. O. Autoxidation of organic compounds in the atmosphere. *J. Phys. Chem. Lett.* **2013**, *4*, 3513–3520.
- (97) Bianchi, F.; Kurtén, T.; Riva, M.; Mohr, C.; Rissanen, M. P.; Roldin, P.; Berndt, T.; Crounse, J. D.; Wennberg, P. O.; Mentel, T. F.; Wildt, J.; Junninen, H.; Jokinen, T.; Kulmala, M.; Worsnop, D. R.; Thornton, J. A.; Donahue, N.; Kjaergaard, H. G.; Ehn, M. Highly Oxygenated Organic Molecules (HOM) from Gas-Phase Autoxidation Involving Peroxy Radicals: A Key Contributor to Atmospheric Aerosol. *Chem. Rev.* **2019**, *119*, 3472–3509.

(98) Tröstl, J.; Chuang, W. K.; Gordon, H.; Heinritzi, M.; Yan, C.; Molteni, U.; Ahlm, L.; Frege, C.; Bianchi, F.; Wagner, R.; Simon, M.; Lehtipalo, K.; Williamson, C.; Craven, J. S.; Duplissy, J.; Adamov, A.; Almeida, J.; Bernhammer, A.-K.; Breitenlechner, M.; Brilke, S.; Dias, A.; Ehrhart, S.; Flagan, R. C.; Franchin, A.; Fuchs, C.; Guida, R.; Gysel, M.; Hansel, A.; Hoyle, C. R.; Jokinen, T.; Junninen, H.; Kangasluoma, J.; Keskinen, H.; Kim, J.; Krapf, M.; Kürten, A.; Laaksonen, A.; Lawler, M.; Leiminger, M.; Mathot, S.; Möhler, O.; Nieminen, T.; Onnela, A.; Petäjä, T.; Piel, F. M.; Miettinen, P.; Rissanen, M. P.; Rondo, L.; Sarnela, N.; Schobesberger, S.; Sengupta, K.; Sipilä, M.; Smith, J. N.; Steiner, G.; Tomè, A.; Virtanen, A.; Wagner, A. C.; Weingartner, E.; Wimmer, D.; Winkler, P. M.; Ye, P.; Carslaw, K. S.; Curtius, J.; Dommen, J.; Kirkby, J.; Kulmala, M.; Riipinen, I.; Worsnop, D. R.; Donahue, N. M.; Baltensperger, U. The role of low-volatility organic compounds in initial particle growth in the atmosphere. *Nature* **2016**, *533*, 527–531.

(99) Ehn, M.; Thornton, J. A.; Kleist, E.; Sipilä, M.; Junninen, H.; Pullinen, I.; Springer, M.; Rubach, F.; Tillmann, R.; Lee, B.; Lopez-Hilfiker, F.; Andres, S.; Acir, I.-H.; Rissanen, M.; Jokinen, T.; Schobesberger, S.; Kangasluoma, J.; Kontkanen, J.; Nieminen, T.; Kurtén, T.; Nielsen, L. B.; Jørgensen, S.; Kjaergaard, H. G.; Canagaratna, M.; Maso, M. D.; Berndt, T.; Petäjä, T.; Wahner, A.; Kerminen, V.-M.; Kulmala, M.; Worsnop, D. R.; Wildt, J.; Mentel, T. F. A large source of low-volatility secondary organic aerosol. *Nature* **2014**, *506*, 476–479.

(100) Mutzel, A.; Poulaire, L.; Berndt, T.; Iinuma, Y.; Rodigast, M.; Böge, O.; Richters, S.; Spindler, G.; Sipilä, M.; Jokinen, T.; Kulmala, M.; Herrmann, H. Highly Oxidized Multifunctional Organic Compounds Observed in Tropospheric Particles: A Field and Laboratory Study. *Environ. Sci. Technol.* **2015**, *49*, 7754–7761.

(101) Pye, H. O. T.; D'Ambro, E. L.; Lee, B. H.; Schobesberger, S.; Takeuchi, M.; Zhao, Y.; Lopez-Hilfiker, F.; Liu, J.; Shilling, J. E.; Xing, J.; Mathur, R.; Middlebrook, A. M.; Liao, J.; Welti, A.; Graus, M.; Warneke, C.; de Gouw, J. A.; Holloway, J. S.; Ryerson, T. B.; Pollack, I. B.; Thornton, J. A. Anthropogenic enhancements to production of highly oxygenated molecules from autoxidation. *Proc. Natl. Acad. Sci. U.S.A.* **2019**, *116*, 6641–6646.

(102) Wang, S.; Wu, R.; Berndt, T.; Ehn, M.; Wang, L. Formation of Highly Oxidized Radicals and Multifunctional Products from the Atmospheric Oxidation of Alkylbenzenes. *Environ. Sci. Technol.* **2017**, *51*, 8442–8449.

(103) Tsiligiannis, E.; Hammes, J.; Salvador, C. M.; Mentel, T. F.; Hallquist, M. Effect of NO<sub>x</sub> on 1,3,5-trimethylbenzene (TMB) oxidation product distribution and particle formation. *Atmos. Chem. Phys.* **2019**, *19*, 15073–15086.

(104) Garmash, O.; Rissanen, M. P.; Pullinen, I.; Schmitt, S.; Kausiala, O.; Tillmann, R.; Zhao, D.; Percival, C.; Bannan, T. J.; Priestley, M.; Hallquist, Å. M.; Kleist, E.; Kiendler-Scharr, A.; Hallquist, M.; Berndt, T.; McFiggans, G.; Wildt, J.; Mentel, T. F.; Ehn, M. Multi-generation OH oxidation as a source for highly oxygenated organic molecules from aromatics. *Atmos. Chem. Phys.* **2020**, *20*, 515–537.

(105) Cheng, X.; Chen, Q.; Jie Li, Y.; Zheng, Y.; Liao, K.; Huang, G. Highly Oxygenated Organic Molecules Produced by the Oxidation of Benzene and Toluene in a Wide Range of OH Exposure and NO<sub>x</sub> Conditions. *Atmos. Chem. Phys.* **2021**, *21*, 12005–12019.